Neuron

Article

SUMOylation of Enzymes and Ion Channels in Sensory Neurons Protects against Metabolic Dysfunction, Neuropathy, and Sensory Loss in Diabetes

Highlights

- Post-translational SUMOylation critically protects sensory neuron function
- SUMOylation regulates bioenergetic enzymes and controls toxic metabolites
- SUMOylation functionally regulates the nociceptive ion channel TRPV1
- De-SUMOylation accelerates progression of diabetic neuropathy

Authors

Nitin Agarwal, Francisco J. Taberner, Daniel Rangel Rojas, ..., Peter P. Nawroth, Gary R. Lewin, Rohini Kuner

Correspondence

rohini.kuner@pharma.uni-heidelberg.de

In Brief

Agarwal et al. show that the post-translational modification of SUMO-conjugation of proteins (SUMOylation) in pain-sensing neurons regulates sensory ion channels and metabolic enzymes governing energy production. Reduced SUMOylation in diabetes leads to metabolic arrest and accumulation of toxic metabolites, driving neuropathy and sensory loss. Enhancing SUMOylation may reverse diabetic neuropathy.

Agarwal et al., 2020, Neuron *107*, 1–19
September 23, 2020
https://doi.org/10.1016/j.neuron.2020.06.037

CellPress

Neuron

CellPress

Article

SUMOylation of Enzymes and Ion Channels in Sensory Neurons Protects against Metabolic Dysfunction, Neuropathy, and Sensory Loss in Diabetes

Nitin Agarwal,[1] Francisco J. Taberner,[1] Daniel Rangel Rojas,[1] Mirko Moroni,[2] Damir Omberbasic,[2] Christian Njoo,[1] Alexandra Andrieux,[3] Pooja Gupta,[1] Kiran K. Bali,[1] Esther Herpel,[4] Faramarz Faghihi,[1] Thomas Fleming,[5] Anne Dejean,[3] Stefan G. Lechner,[1] Peter P. Nawroth,[5] Gary R. Lewin,[2] and Rohini Kuner[1,6,*]

[1]Pharmacology Institute, Heidelberg University, Im Neuenheimer Feld 366, 69120 Heidelberg, Germany

[2]Molecular Physiology of Somatic Sensation, Department of Neuroscience, Max-Delbrück Centre for Molecular Medicine, Robert-Rössle Straße 10, 13092 Berlin, Germany

[3]Nuclear Organization and Oncogenesis Unit, INSERM U993, Institute Pasteur, 75015 Paris, France

[4]Institute of Pathology, Heidelberg University, Im Neuenheimer Feld 224, 69120 Heidelberg, Germany

[5]Medical Clinic Heidelberg, Department of Medicine I and Clinical Chemistry, University Hospital of Heidelberg, Heidelberg University, INF 410, 69120 Heidelberg, Germany

[6]Lead Contact

*Correspondence: rohini.kuner@pharma.uni-heidelberg.de

https://doi.org/10.1016/j.neuron.2020.06.037

SUMMARY

Diabetic peripheral neuropathy (DPN) is a highly frequent and debilitating clinical complication of diabetes that lacks therapies. Cellular oxidative stress regulates post-translational modifications, including SUMOylation. Here, using unbiased screens, we identified key enzymes in metabolic pathways and ion channels as novel molecular targets of SUMOylation that critically regulated their activity. Sensory neurons of diabetic patients and diabetic mice demonstrated changes in the SUMOylation status of metabolic enzymes and ion channels. In support of this, profound metabolic dysfunction, accelerated neuropathology, and sensory loss were observed in diabetic gene-targeted mice selectively lacking the ability to SUMOylate proteins in peripheral sensory neurons. TRPV1 function was impaired by diabetes-induced de-SUMOylation as well as by metabolic imbalance elicited by de-SUMOylation of metabolic enzymes, facilitating diabetic sensory loss. Our results unexpectedly uncover an endogenous post-translational mechanism regulating diabetic neuropathy in patients and mouse models that protects against metabolic dysfunction, nerve damage, and altered sensory perception.

INTRODUCTION

Diabetes is one of the most highly prevalent disorders with an incidence of more than 8% in adults. In diabetes, endogenous defense systems are overwhelmed, leading to various types of stress and microvascular complications, such as nephropathy, retinopathy, and neuropathy (Lim, 2014; Duh et al., 2017; Boulton et al., 2005). Diabetic peripheral neuropathy (DPN) affects approximately 21% of patients with diabetes (Tesfaye and Seaquist, 2004; Nawroth et al., 2017), is a leading cause of neuropathic pain and foot ulceration, and is primarily responsible for leg amputations. Consequently, DPN is linked to a significant reduction in quality of life and mortality in diabetic patients.

Our understanding of the molecular mechanisms underlying DPN is still in its infancy because the majority of studies are focused on the underpinnings of neuropathic pain associated with physical nerve trauma. Diabetes-induced nerve damage is highly diffuse, follows a variable course, and is tightly linked to the extent of metabolic dysfunction and generation of reactive oxygen species (ROS) (Feldman et al., 2017). Recent studies suggest that ROS and oxidative stress regulate key cellular processes via post-translational modifications such as ubiquitination, acetylation, nitrosylation, glycation, and **linked β- -acetl-glucosamin** ((O-GlcNAcylation), which have been implicated in late complications of diabetes (McLaughlin et al., 2016; Forbes and Cooper 2013).

Covalent modification by small ubiquitin-related modifier (SUMO) polypeptides (a process called SUMOylation) is a more recently described form of post-translational modification that enables rapid cellular response to dynamic changes in signals (Geiss-Friedlander and Melchior, 2007; Martin et al., 2007). SUMOylation is characterized by covalent attachment of SUMO moieties to lysines on substrate proteins, leading to profound regulation of protein localization or function (Geiss-Friedlander and Melchior, 2007; Martin et al., 2007). SUMO proteins are small (approximately 11 kDa), and modification via SUMO binding is covalent and reversible. Although the diverse steps underlying SUMOylation involve several enzymes, the role of the E2

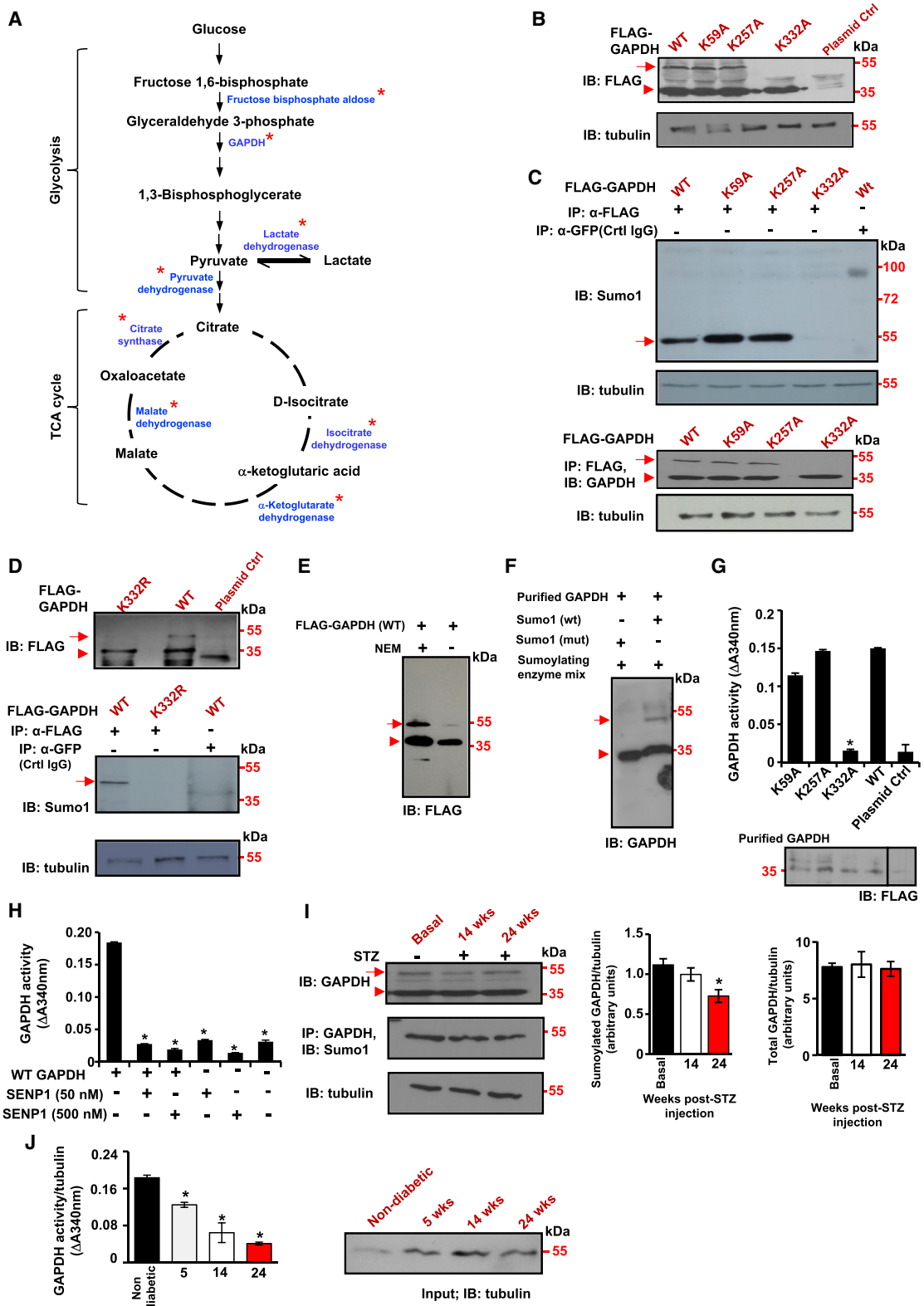

(legend on next page)

conjugating enzyme is solely taken up by Ubc9; therefore, loss of Ubc9 precludes SUMOylation (Nacerddine et al., 2005). SUMOylation has a protective role in stroke and brain ischemia (Silveirinha et al., 2013; Krajnak and Dahl, 2018), whereas it has been suggested to contribute to the pathophysiology of some neurodegenerative disorders, such as Parkinson's disease (Yau et al., 2020) and polyglutamine androgen receptor-mediated disease (Chua et al., 2015), indicating that a fine balance between SUMOylated and un-SUMOylated proteins is essential. SUMOylation has been implicated in pancreatic etiology of diabetes (Li et al., 2005; Dai et al., 2011). However, nothing is known about its role with respect to neurodegeneration or neuroprotection in DPN. Because metabolic imbalance and oxidative stress in diabetes are known to trigger and be worsened by post-translational modifications of proteins (Zheng et al., 2016), and SUMOylation particularly has been linked to oxidative stress in the tissue environment (de la Vega et al., 2012; Yang et al., 2014), we hypothesized a role of SUMOylation in neurological complications of diabetes, including pain and DPN.

By performing SUMO proteomics on sensory neurons and nerves, we find that SUMOylation targets a number of important metabolic enzymes and ion channels in peripheral sensory neurons, profoundly alters their functions, and is highly altered in nerves of diabetic mice and diabetic patients undergoing amputation. By generating mice specifically lacking SUMOylation in peripheral sensory neurons, we report a key neuroprotective role of SUMOylation against bioenergetic crises that lead to sensory loss in diabetes. Our results clarify the fundamental underpinnings of molecular processes underlying hyperglycemia-induced metabolic plasticity in neurons and lay a basis for designing new therapeutic options.

RESULTS

Key Metabolic Enzymes are SUMOylated in DRG Neurons

We set out to identify novel protein targets of SUMOylation in sensory neurons of mouse dorsal root ganglia (DRGs) via proteomics/liquid chromatography-tandem mass spectrometry (LC-MS and MS) analyses upon protein pull-down with an anti-SUMO1 antibody or anti-GFP antibody as a control and subsequently validate prioritized targets in molecular and functional studies. Upon including several biological replicates and stringent statistical analyses (STAR Methods), we identified 169 proteins as putative targets of SUMO modification from DRG lysates (Table S1) that included neuronal and non-neuronal proteins and shortlisted salient targets based on their putative functions in metabolism, generation of advanced glycation products, and potential role in sensory defects (Table S2). Performing the screen quantitatively on DRGs of naive mice and streptozotocin (STZ)-injected mice 5 weeks post-STZ indicated that several targets could be differentially pulled down from DRGs with the anti-SUMO antibody, suggesting that SUMOylation is regulated by diabetes (Table S3). A number of key enzymes in metabolic pathways, including the glycolysis pathway and the Krebs cycle (tricarboxylic acid [TCA] cycle), emerged as putative targets of SUMOylation (marked by an asterisk in Figure 1A; Figure S1). Furthermore, key enzymes from the pentose phosphate pathway, enzymes affecting nicotinamide adenine dinucleotide oxidized and reduced form (NAD^+/NADH) balance, and those involved in detoxification processes were also identified. Among these, we validated glyceraldehyde 3-phosphate dehydrogenase (GAPDH), citrate synthase, transketolase-like protein-1 (TKTL1), and aldehyde dehydrogenase isoform α-3A1 (ALDH3A1) with respect to SUMOylation and modulation of function by SUMOylation, as described below.

SUMOylation Is Required for Activity of GAPDH in DRG Neurons and Attenuated in Mice with Diabetes

We assigned a high priority to GAPDH because inactivation of GAPDH has been implicated in formation of advanced glycation products in other late complications of diabetes (Nishikawa et al., 2000; Madsen-Bouterse et al., 2010; Kanwar and Kowluru 2009). *In silico* analyses led to prediction of 3 potential SUMOylation sites in the GAPDH protein (lysines at positions 59, 257, and 332; Figure S2A), which we mutated using site-directed mutagenesis to alanines (K59A, K257A, and K332A, respectively) in constructs expressing FLAG tagged-GAPDH. Immunoblotting of lysates of transfected HEK cells indicated the presence of un-SUMOylated (arrowhead, Figure 1B) and SUMOylated GAPDH (arrow, Figure 1B) in cells expressing the K59A, K257A, and wild-type versions of GAPDH, whereas cells

Figure 1. Identification of SUMOylated Proteins in Sensory Neurons of the Dorsal Root Ganglia (DRGs) and Molecular and Functional Validation of Glyceraldehyde 3-Phosphate Dehydrogenase (GAPDH) as a SUMOylation Target

(A) Overview of enzymes in the glycolysis pathway and tricarboxylic acid (TCA) cycle that were identified to be regulated by SUMOylation (asterisk).

(B) Immunoblotting (IB) analysis from FLAG-tagged GAPDH and diverse mutants.

(C) Immunoblotting and immunoprecipitation (IP) studies from FLAG-tagged GAPDH and diverse mutants of potentially SUMOylated lysines mutated to alanine expressed in HEK cells, using tubulin expression as a loading control.

(D) IB and IP studies from FLAG-tagged GAPDH and mutant of potentially SUMOylated lysines mutated to arginine expressed in HEK cells, using tubulin expression as a loading control.

(E) Change in proportion of SUMOylated GAPDH in the presence or absence of the de-SUMOylation inhibitor NEM.

(F) *In vitro* SUMOylation assay performed on purified GAPDH.

(G and H) *In vitro* GAPDH activity assay on purified proteins (the bottom panel in G shows the purified protein) or on lysates of HEK cells expressing WT GAPDH and treated with the SUMO-specific isopeptidase SENP1 or a control.

(I) Levels of SUMOylated GAPDH or total GAPDH (quantified over tubulin) in DRGs of control mice and mice at 14 weeks or 24 weeks in the streptozotocin (STZ) model.

(J) GAPDH activity assay on DRGs of control mice and mice 5 weeks, 14 weeks, or 24 weeks post-STZ.

Arrows and arrowheads denote the SUMOylated and un-SUMOylated forms of GAPDH, respectively. n = 3 independent experiments or 3 mice/genotype/condition. *$p < 0.05$, ANOVA for random measures followed by Tukey's test. Data represent mean ± SEM.

Please cite this article in press as: Agarwal et al., SUMOylation of Enzymes and Ion Channels in Sensory Neurons Protects against Metabolic Dysfunction, Neuropathy, and Sensory Loss in Diabetes, Neuron (2020), https://doi.org/10.1016/j.neuron.2020.06.037

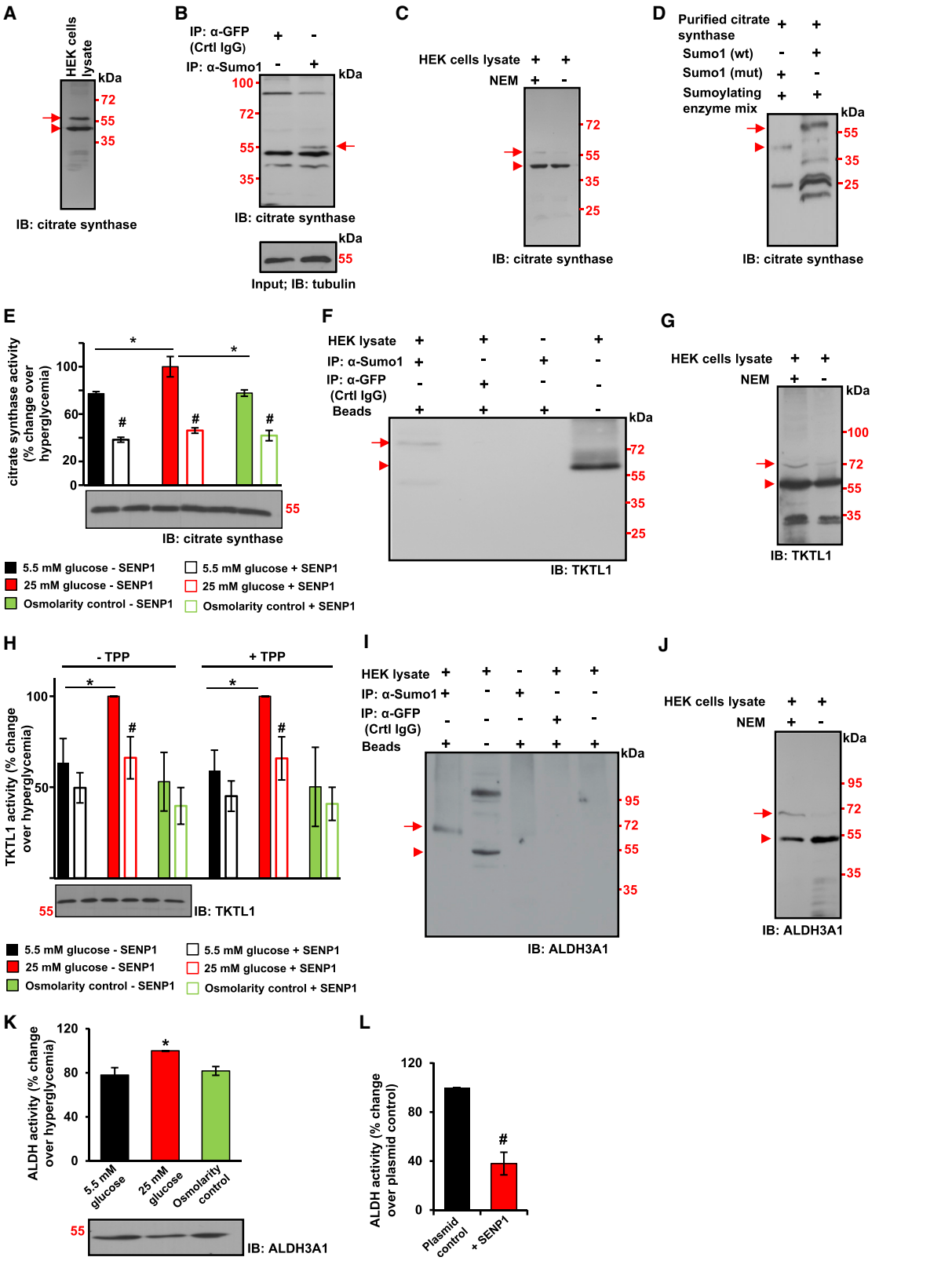

(legend on next page)

Please cite this article in press as: Agarwal et al., SUMOylation of Enzymes and Ion Channels in Sensory Neurons Protects against Metabolic Dysfunction, Neuropathy, and Sensory Loss in Diabetes, Neuron (2020), https://doi.org/10.1016/j.neuron.2020.06.037

expressing the GAPDH mutant K332A lacked the SUMOylated protein (arrow in Figure 1B), indicating that lysine 332 is a potential SUMOylation site in GAPDH. Upon immunoprecipitating the protein with an anti-FLAG antibody and immunoblotting with a SUMO-1 antibody, we confirmed that SUMOylation of GAPDH occurs on lysine 332 (Figure 1C, top panel). Similarly, immunoprecipitating the protein with an anti-FLAG antibody and immunoblotting with an anti-GAPDH1 antibody (Figure 1C, bottom panel) revealed the presence of SUMOylated (arrow) and non-SUMOylated (arrowhead) GAPDH in cells expressing K59A, K257A, and wild-type versions of GAPDH, whereas cells expressing the GAPDH mutant K332A only showed the non-SUMOylated protein (arrowhead). To further verify the specificity of SUMOylation at K332, we generated a K332R mutant and again observed lack of expression (Figure 1D, top panel) or lack of immunoprecipitation (Figure 1D, bottom panels) of the SUMOylated fraction. Furthermore, during immunoprecipitation of FLAG-tagged GAPDH in HEK cells, the band corresponding to the SUMOylated fraction (arrow in Figure 1E) was readily detected in the presence of N-ethylmaleimide (NEM), an inhibitor of cysteine peptidases that de-SUMOylate proteins, and reduced when NEM was excluded during the experiment (Figure 1E). Finally, we further verified GAPDH SUMOylation by performing *in vitro* SUMOylation on purified GAPDH protein (Figure 1F). In all experiments described above, the shift in band size corresponding to SUMOylation was on the order of 12–15 kDa; i.e., indicative of mono-SUMOylation. We next sought to address how SUMOylation is linked to the catalytic activity of GAPDH. We purified wild-type GAPDH and the SUMOylation-deficient mutant K332A GAPDH proteins and observed that activity of the de-SUMOylation mutant was significantly lower than that of wild-type GAPDH (Figure 1G). Treating wild-type GAPDH with SENP-1, a SUMO-specific isopeptidase that de-SUMOylates proteins (Witty et al., 2010), led to decreased GAPDH activity (Figure 1H).

In vivo quantitative analyses showed that the levels of GAPDH immunoprecipitated with anti-SUMO1 drop markedly at late stages post-STZ (significantly 24 weeks post-STZ; Figure 1I), although there was no overall decrease in GAPDH expression (Figure 1I). This was accompanied by a decrease in GAPDH activity in DRG lysates of STZ-treated mice starting 14 weeks post-STZ (Figure 1J).

SUMOylation Targets Citrate Synthase, TKTL1, and α-ALDH3A1 and Is Required for Elevation of Their Activity under Conditions of Hyperglycemia

In HEK cells, anti-SUMO1, but not control anti-GFP immunoglobulin G (IgG), immunoprecipitated an extra, higher-molecular-weight band corresponding to citrate synthase mono-SUMOylated at its 55-kDa form (arrow in Figure 2B). SUMOylation was reduced in the absence of NEM (Figure 2C), and mono-SUMOylation was further confirmed via an *in vitro* SUMOylation assay performed on purified citrate synthase (Figure 2D). In activity assays, citrate synthase showed elevated activity when HEK cells were grown in high-glucose concentration (25 mM) compared with 5.5 mM glucose (Figure 2E). As a control, substituting high glucose with an equal measure of mannitol, which also increases osmolarity like glucose, did not lead to elevated citrate synthase activity (Figure 2E). Co-expression of SENP1 reduced the basal catalytic activity of citrate synthase and hyperglycemia-induced elevation (Figure 2E).

In HEK cells, an anti-TKTL1 immunoreactive band of 72 kDa was detected (arrow in Figure 2F) in addition to the de-SUMOylated form of lower molecular weight (arrowhead in Figure 2F), suggesting mono-SUMOylation. SUMOylation was reduced in the absence of NEM (Figure 2G). Regardless of the presence or absence of its co-factor thiamine pyrophosphate (TPP), the activity of TKTL1 was increased significantly in HEK cells exposed to 25 mM glucose compared with 5.5 mM glucose or 5.5 mM glucose and 19.5 mM mannitol (Figure 2H). De-SUMOylation via SENP1 abrogated the hyperglycemia-induced increase in TKTL1 activity (Figure 2H; loading controls are shown in Figure 2E).

Bands corresponding to endogenous expression of ALDH3A1 in HEK cells were found below 55 kDa and just above 95 kDa. Immunoprecipitation with an anti-SUMO1 antibody yielded a single major band at around 72 kDa, indicating mono-SUMOylation (Figure 2I). The band shift did not occur in the absence of NEM (Figure 2J). Pan-ALDH activity was significantly elevated in HEK cells exposed to 25 mM glucose compared with 5.5 mM glucose

Figure 2. Validation of Citrate Synthase, Transketolase-like Protein 1 (TKTL1), and the Aldehyde Dehydrogenase Isoform ALDH3A1 as SUMOylation Targets and Modulation of Activity by SUMOylation and Exposure to High Glucose (25 mM) or Normal Glucose (5.5 mM + 19.5 mM Mannitol)

(A and B) IB of endogenous citrate synthase in HEK cells (A) and IP with an anti-SUMO1 antibody but not an anti-GFP antibody (control IgG; B).
(C) Change in the proportion of SUMOylated citrate synthase in the presence or absence of NEM.
(D) *In vitro* SUMOylation assay performed on purified citrate synthase.
(E) *In vitro* citrate synthase activity assay performed on lysates of HEK cells transfected with a plasmid expressing SENP1 or a control vector.
(F) IP of endogenous TKTL1 in HEK cells with an anti-SUMO1 antibody but not an anti-GFP antibody.
(G) Change in proportion of SUMOylated TKTL1 in the presence or absence of NEM.
(H) *In vitro* TKTL1 activity assay performed on HEK cells expressing SENP1 or a control vector in the presence or absence of the cofactor thiamine pyrophosphate (TPP). Values are normalized, taking the high-glucose condition as 100%.
(I) IP of endogenous ALDH3A1 in HEK cells with an anti-SUMO1 antibody but not an anti-GFP antibody.
(J) Change in proportion of SUMOylated ALDH3A1 in the presence or absence of NEM.
(K and L) *In vitro* pan-aldehyde dehydrogenase (ALDH) activity assay performed on HEK cells (K) and the effect of SENP1 (L). Values are normalized, taking the high-glucose condition as 100%.
Arrows and arrowheads indicate SUMOylated and un-SUMOylated forms of proteins, respectively. n = at least 3 independent culture experiments. Tubulin IB was employed as a control for protein expression in all quantitative analyses. *$p < 0.05$ compared with values in normal glucose and #$p < 0.05$ compared with the corresponding control-transfected group. Data represent mean ± SEM.

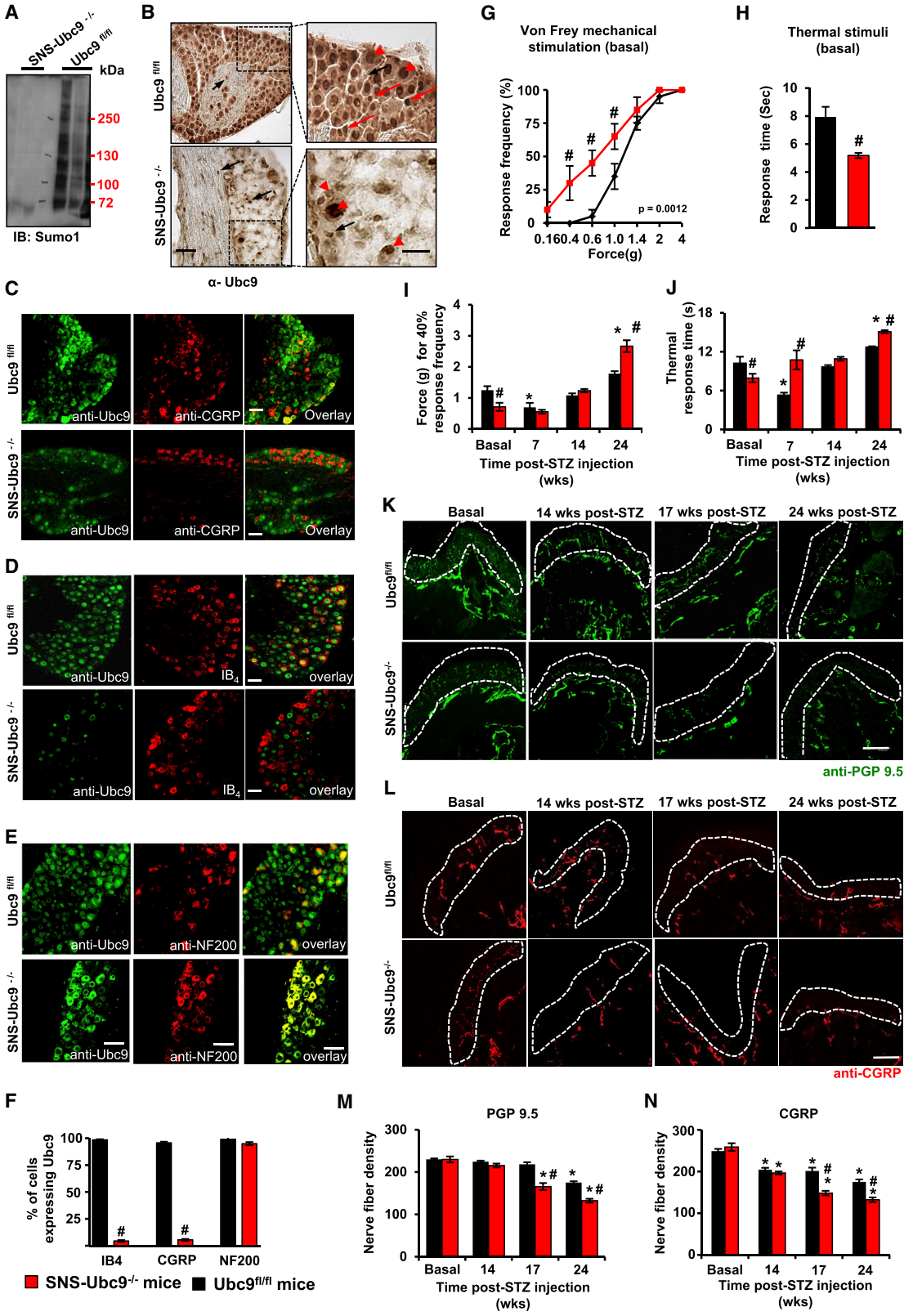

(legend on next page)

Please cite this article in press as: Agarwal et al., SUMOylation of Enzymes and Ion Channels in Sensory Neurons Protects against Metabolic Dysfunction, Neuropathy, and Sensory Loss in Diabetes, Neuron (2020), https://doi.org/10.1016/j.neuron.2020.06.037

(Figure 2K; loading controls are also shown in Figure 2K) or 5.5 mM glucose and 19.5 mM mannitol. Cells coexpressing SENP1 showed a significant decrease in ALDH activity (Figure 2L). Thus, each of the 4 targets we prioritized from the list of SUMOylation targets identified in the anti-SUMO1 immunoprecipitation screen could be substantiated as *bona fide* substrates for molecular as well as functional regulation via SUMOylation, suggesting high accuracy and validity of our unbiased screen.

Mice Lacking SUMOylation Specifically in Sensory Neurons Demonstrate Exaggerated Neuropathology and Sensory Loss in Diabetic Neuropathy

To address the functional significance of SUMOylation in peripheral sensory neurons, we generated mice lacking the ability to SUMOylate proteins in DRG neurons (*SNS-Ubc9*$^{-/-}$ mice; Figure S2B). Immunoblotting with an anti-SUMO1 antibody showed complete lack of bands in DRGs of *SNS-Ubc9*$^{-/-}$ mice, whereas DRGs of control Ubc9$^{fl/fl}$ mice showed a major smear representing the multitude of proteins that are SUMOylated in DRG cells under wild-type conditions (Figure 3A). Immunohistochemical staining with the anti-Ubc9 antibody (negative controls are shown in Figure S2C) confirmed loss of Ubc9 expression in small-diameter neurons in DRGs of *SNS-Ubc9*$^{-/-}$ mice (Figure 3B; arrows in high-magnification images shown on the right), whereas staining was preserved in large-diameter neurons and Schwann cells (Figure 3B; arrowheads in high-magnification images). Co-immunofluorescence analysis showed that, although nearly all non-peptidergic (IB4-binding; Figure 3D) and peptidergic nociceptive neurons (anti-calcitonin gene-related peptide [CGRP]-immunoreactive; Figure 3C) expressed Ubc9 in control mice, *SNS-Ubc9*$^{-/-}$ mice demonstrated lack of co-labeling (see quantification in Figure 3F). In contrast, co-immunofluorescence with neurofilament 200 (NF200) demonstrated comparable number of large-diameter, non-nociceptive neurons co-stained with anti-Ubc9 in *SNS-Ubc9*$^{-/-}$ mice and control Ubc9$^{fl/fl}$ mice (Figures 3E and 3F), indicating the specificity of gene deletion expected from the SNS-Cre line (Agarwal et al., 2004).

We then conducted behavioral analyses to test the responsivity of mice lacking SUMOylation in DRG neurons to somatosensory stimuli. Compared with Ubc9$^{fl/fl}$ mice, *SNS-Ubc9*$^{-/-}$ mice showed a significantly higher frequency of withdrawal responses to mechanical force applied via von Frey filaments to the plantar hindpaw surface (Figure 3G) and shortened latency of withdrawal to plantar application of noxious infrared heat (Figure 3H), indicating that basal nociception is enhanced upon loss of SUMOylation in sensory neurons. We then addressed the effect of de-SUMOylation in sensory neurons on DPN in longitudinal analyses that encompassed 7, 14, and 24 week post-STZ injection; i.e., time points that are temporally largely separated from any potential acute toxic effects of STZ (Koulmanda et al., 2003) and spanned the characteristic biphasic temporal nature of early nociceptive hypersensitivity (Agarwal et al., 2018). *SNS-Ubc9*$^{-/-}$ mice were indistinguishable from Ubc9$^{fl/fl}$ mice at the early phase of diabetic nociceptive hypersensitivity but developed more profound mechanical hypoalgesia (Figure 3I) and accelerated thermal hypoalgesia (Figure 3J) compared with Ubc9$^{fl/fl}$ mice at chronic stages post-STZ, showing an accelerated course of DPN in the absence of SUMOylation. Immunostaining for the pan-nerve antigen PGP9.5 (Figure 3K) and a nociceptive peptidergic marker (CGRP; Figure 3L) on paw skin sections at distinct time points until 24 weeks post-STZ revealed that, although nerve density was comparable in *SNS-Ubc9*$^{-/-}$ and Ubc9$^{fl/fl}$ mice under naive conditions, DPN-associated loss of epidermal nerve fibers, particularly nociceptive fibers, was accelerated in SUMOylation-deficient mice (see examples in Figures 3K and 3L and quantitative summary in Figures 3M and 3N, respectively). Thus, behavioral and morphological data show that loss of SUMOylation in sensory neurons leads to an exaggerated magnitude and faster progression of DPN.

SUMOylation Regulates Major Metabolic Pathways in Peripheral Sensory Neurons

In GAPDH activity assays on DRGs, *SNS-Ubc9*$^{-/-}$ mice showed significantly reduced basal GAPDH activity and a higher magnitude of diabetes-induced decrease in GAPDH activity compared with Ubc9$^{fl/fl}$ mice (Figure 4A). Thus, impairment of GAPDH activity by de-SUMOylation is exacerbated further under diabetic conditions.

In LC-MS analyses, consistent with impairment of GAPDH activity upon loss of SUMOylation, diabetic *SNS-Ubc9*$^{-/-}$ mice demonstrated exaggerated accumulation of the GAPDH

Figure 3. Characterization of Mice Lacking SUMOylation in Peripheral Nociceptive Neurons (*SNS-Ubc9*$^{-/-}$) or Control Littermates (Ubc9$^{fl/fl}$) and Analysis of the Course of Diabetic Neuropathy (DPN) via Neuropathological and Behavioral Assays

(A) Western blot analysis of DRG lysates of *SNS-Ubc9*$^{-/-}$ mice and control Ubc9$^{fl/fl}$ littermates with an anti-SUMO1 antibody.

(B) Representative images of immunohistochemistry with an anti-SUMO1 antibody on DRGs. Red arrows indicate labeled small-diameter neurons, red arrowheads indicate labeled large-diameter neurons, and black arrows represent labeled Schwann cells. Scale bars represent 75 μm and 40 μm in the left and right panels, respectively.

(C–F) Expression of Ubc9 in DRG neurons labeled immunohistochemically for calcitonin gene-related peptide (CGRP; peptidergic nociceptors, C) binding to Isolectin-B4 (IB_4; non-peptidergic nociceptors, D) or neurofilament 200 (NF200; large-diameter neurons, E). Typical examples (C–E) and quantitative summary of co-labeling (F) are shown. N = 4 mice/genotype.

(G and H) Basal plantar sensitivity of adult mice to mechanical stimuli (von Frey hairs, G) and a heat ramp (Hargreaves test, H). N = 8 mice/genotype. The p value in (G) represents statistical comparison of the two stimulus-response curves. In (H), #$p < 0.05$ between genotypes, Student's t test.

(I and J) Summary of response thresholds and thermal latency before and after STZ injection (n = 12 mice per genotype). *$p < 0.05$ compared with basal values, #$p < 0.05$ between genotypes, ANOVA of repeated measures, post hoc Tukey's test.

(K–N) Typical examples (K and L) and quantitative intensity measurements (M and N) of nerve endings in the plantar epidermis (demarcated by dashed lines) prior to and over 24 weeks post-STZ, immunoreactive for anti-PGP9.5 (K; scale bar, 60 μm) or anti-CGRP (L; scale bar, 25 μm). *$p < 0.05$ compared with basal, #$p < 0.05$ between genotypes, ANOVA of repeated measures, post hoc Tukey's test.

Data represent mean ± SEM.

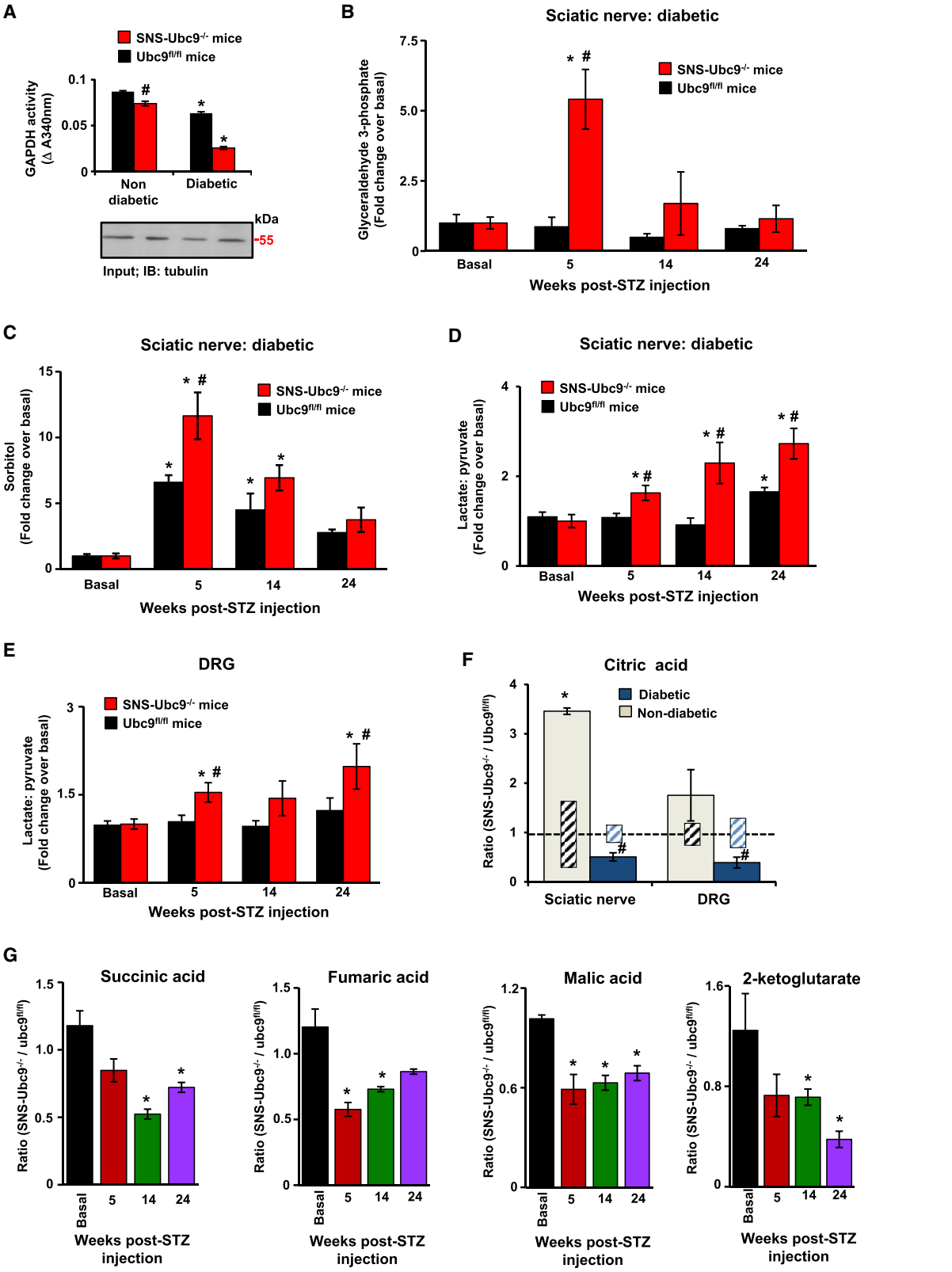

(legend on next page)

Please cite this article in press as: Agarwal et al., SUMOylation of Enzymes and Ion Channels in Sensory Neurons Protects against Metabolic Dysfunction, Neuropathy, and Sensory Loss in Diabetes, Neuron (2020), https://doi.org/10.1016/j.neuron.2020.06.037

substrate glyceraldehyde 3-phosphate between 5–14 weeks post-STZ compared with diabetic Ubc9$^{fl/fl}$ mice (Figure 4B). Because GAPDH activity remains impaired until 24 weeks, the normalization of glyceraldehyde 3-phosphate levels is likely attributable to defects in the enzymes that generate glyceraldehyde 3-phosphate, consistent with our identification of fructose biphosphate aldose or transketolase (Figure S1) as SUMOylation targets. This would suggest that, in mice lacking SUMOylation, the metabolites are preferentially passed through pathways generating harmful metabolites, such as the polyol pathway (Yagihashi et al., 2011). In support of this, sorbitol levels surged in sciatic nerve biopsies of diabetic *SNS-Ubc9*$^{-/-}$ mice between 5–14 weeks over baseline values to a significantly higher extent than in diabetic Ubc9$^{fl/fl}$ mice (Figure 4C). Farther along the glycolysis pathway, pyruvate levels were significantly decreased, whereas L-lactate levels were increased, in sciatic nerve biopsies (Figure 4D) and DRG somata (Figure 4E) of *SNS-Ubc9*$^{-/-}$ mice compared with control Ubc9$^{fl/fl}$ mice post-STZ but not under basal conditions. The diabetes-induced increase in the lactate-to-pyruvate ratio, which is taken as an indicator of disorder in the respiratory chain and TCA cycle (Poggi-Travert et al., 1996), was accelerated drastically in *SNS-Ubc9*$^{-/-}$ mice (starting at 5 weeks post-STZ) in comparison with Ubc9$^{fl/fl}$ mice (starting at 24 weeks post-STZ) (Figures 4D and 4E).

Citric acid levels were increased in *SNS-Ubc9*$^{-/-}$ mice compared with those in Ubc9$^{fl/fl}$ mice under basal (non-diabetic) conditions, but following STZ-induced diabetes, citric acid was depleted significantly in peripheral sensory neurons and axons of *SNS-Ubc9*$^{-/-}$ mice compared with Ubc9$^{fl/fl}$ mice (Figure 4F). The metabolites from successive steps in the TCA cycle, including isocitric acid, 2-ketoglutarate (2KG), succinic acid, and fumaric acid were found at lower levels in the sciatic nerve (Figure 4G) and/or DRG somata (Figure S5) of *SNS-Ubc9*$^{-/-}$ mice compared with those in Ubc9$^{fl/fl}$ mice, particularly under diabetic conditions. Thus, these results show that impairment of SUMOylation in sensory neurons leads to buildup of the toxic metabolites sorbitol and lactate while decreasing flux through the TCA cycle.

Although some key neuronal ion channels have been revealed to be profoundly modulated by SUMOylation (Martin et al., 2007; Benson et al., 2007), it became evident that our SUMO proteome screen preferentially uncovered intracellular targets, sparing membrane proteins, likely because of the solubilization conditions we employed. Therefore, we employed a parallel strategy based on *in silico* screening and found SUMOylation sites predicted with a high score in several channels that have been implicated in pain disorders, including diverse sodium channels, potassium channels, and channels of the transient receptor potential (TRP) family (see Table S4 for a complete list). Among these, we studied the cation ion channel TRPV1, which transduces heat, protons, and a variety of algogens (Caterina and Julius, 2001; Patapoutian et al., 2009), in detail. Because TRPV1 is critical for dysfunction of thermal nociception in diabetes (Hong and Wiley, 2005; Pabbidi et al., 2008) and is modulated by metabolites (Kahya et al., 2017; Gram et al., 2017), we hypothesized that modulation of TRPV1 via SUMOylation is mechanistically involved in diabetic complications in sensory neurons. A specific anti-TRPV1 antibody (a kind gift from D. Julius) yielded two bands just below and above 100 kDa (un-SUMOylated TRPV1 is predicted to be 95 kDa) (Figure 5A, input, right). Anti-TRPV1 pulled down a band just larger than 100 kDa that was immunopositive for anti-SUMO1, consistent with the expected shift in mass via covalent linking to several SUMO moieties (Figure 5A, left, top panel). Furthermore, the anti-SUMO1 antibody, but not a control anti-GFP IgG, pulled down TRPV1 at the same molecular size, consistent with this being the SUMOylated form (Figure 5A, bottom left panel).

The SUMOsp 2.0 algorithm predicted 2 putative SUMOylation sites in rat TRPV1 (rTRPV1): at lysine 324, which is situated close to the Ankyrin repeats in the N terminus, and lysine 822, which is situated in C terminus (Figure S3A). Therefore, in HEK cells, we heterologously expressed a construct expressing an N-terminally hemagglutinin (HA)-tagged version of rTRPV1 and co-expressing EGFP to aid identification and mutated lysine 324 or lysine 822 or both to alanine. In a surface biotinylation assay to identify rTRPV1 at the cell surface (Figure 5B, left; loading controls are also shown in Figure 5B), immunoprecipitation with anti-biotin selectively pulled down SUMOylated rTRPV1 (size just larger than 100 kDa) in cells expressing wild-type rTRPV1 or the K822A-TRPV1 mutant but not in cells expressing the K324A mutant or the K324A-K822A double mutant of rTRPV1, whereas the 95-kDa band corresponding to un-SUMOylated rTRPV1 was pulled down in cells expressing all 4 constructs (Figure 5B, left panel). The SUMOylated nature of the upper band was confirmed via anti-SUMO1 immunoblotting after pull-down with the anti-HA antibody (Figure 5B, right panel). These data suggest that rTRPV1 is SUMOylated on lysine 324 but not on lysine 822. The SUMOylated fraction of rTRPV1 was readily detected in the presence of NEM and reduced when NEM was excluded during the experiment (Figure S3E). We further verified SUMOylation by making additional mutations in residues neighboring lysine 324 in the SUMOylation consensus motif: L323A, L325Y, K324R, and E326A (Figure 5C; Figure S3B). As expected for a true SUMOylation consensus motif (Bernier-Villamor et al., 2002), the L323A and L325Y mutations did not affect rTRPV1 SUMOylation, whereas the K324R and E326A mutations abrogated SUMOylation (Figure 5C; loading controls are also shown

Figure 4. Metabolic Status of Sciatic Nerves and DRGs of STZ-Treated and Age-Matched Non-diabetic *SNS-Ubc9*$^{-/-}$ and Ubc9$^{fl/fl}$ mice

(A) *In vitro* estimation of GAPDH activity in DRG lysates 14 weeks post-STZ or controls, normalized to protein input via tubulin expression; N = 4 samples/genotype/group, ANOVA of random measures followed by post hoc Tukey's test.

(B and C) LC-MS-based estimation of glyceraldehyde 3-phosphate (B) and sorbitol (C) in sciatic nerve biopsies.

(D–F) LC-MS-based estimation of lactate:pyruvate ratios (D and E) and citric acid (F) in sciatic nerve biopsies (D and F) and DRGs (E and F).

(G) Estimation of TCA metabolites in sciatic nerves. Data are shown as ratios of levels between *SNS-Ubc9*$^{-/-}$ and control Ubc9$^{fl/fl}$ mice under non-diabetic and diabetic conditions.

For panels (B)–(G), N = 4 samples/genotype/group. *$p < 0.05$ compared with basal ratios, #$p < 0.05$ when compared across genotypes for the same treatment; ANOVA of random measures followed by post hoc Tukey's test. Data represent mean ± SEM.

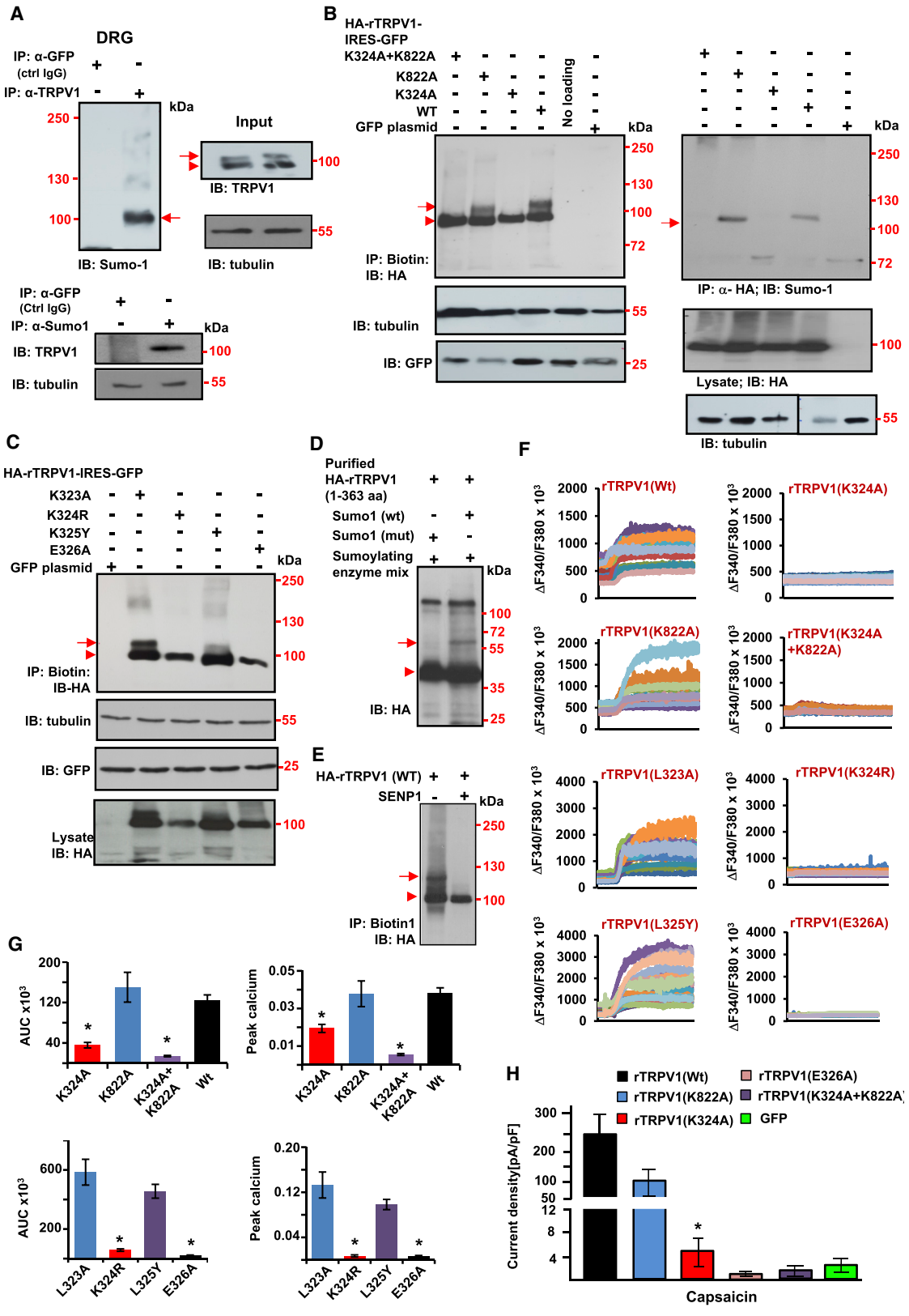

(legend on next page)

in Figure 5C). Furthermore, we generated and purified truncated proteins corresponding to the N-terminal amino acids 1–363 of HA-tagged rTRPV1 and found, in an *in vitro* SUMOylation assay, an additional band for SUMOylated rTRPV1 in samples containing the wild-type functional SUMO1 protein but not in samples containing a dysfunctional mutant form of the SUMO1 protein (Figure 5D). Similar results were obtained when full-length HA-tagged rTRPV1 purified protein was used in an *in vitro* SUMOylation assay (Figure S3F). Finally, *in vitro* treatment of heterologously expressed full-length rTRPV1 with SENP1 led to loss of the band corresponding to SUMOylated TRPV1 (Figure 5E). These converging lines of experiments are direct evidence of TRPV1 SUMOylation.

In Fura2-based calcium imaging assays, exposure to the selective TRPV1 agonist capsaicin (1 μM dose) evoked calcium transients in cells transfected with wild-type rTRPV1 or the K822A, L323A, and L325A mutant forms of rTRPV1 but not in cells expressing the K324A, K324A-K822A, K324R, or E326A mutant forms of TRPV1 (see examples and quantitative summary in Figures 5F and 5G), entirely consistent with the SUMOylation pattern. Identical results were obtained when we comprehensively tested TRPV1-mediated currents in each of the above mutant forms of rTRPV1 in a patch-clamp analysis in transfected HEK cells (Figure 5H). These differences did not arise because of changes in cell surface targeting of any of the above mutant forms of rTRPV1, all of which were found at the cell membrane (see Figures S3C and S3D for details). These results suggest that SUMOylation at lysine 324 is critical for the functionality of TRPV1.

SUMOylation Positively Regulates TRPV1 Function in Sensory Neurons *In Vivo* and Is Reduced under Diabetic Conditions

In the native state, proteins are found in a mixture of SUMOylated and de-SUMOylated forms, and the latter often represents the smaller fraction (Johnson, 2004; Geiss-Friedlander and Melchior, 2007; Sacher et al., 2005). Therefore, we studied the functional role of SUMOylation on TRPV1 channels in their native form in mouse sensory neurons and found that, although significant impairment of TRPV1 function was observed in *SNS-Ubc9*$^{-/-}$ mice, the phenotype was milder than the complete loss of function seen in heterologously expressed TRPV1. In Fura2 imaging studies, although peak calcium transients were comparable across genotypes, the duration of calcium transients was significantly shorter in *SNS-Ubc9*$^{-/-}$ mice than in Ubc9$^{fl/fl}$ mice (Figure 6A). This resulted in a net decrease in calcium flux elicited by capsaicin in sensory neurons of *SNS-Ubc9*$^{-/-}$ mice, whereas KCl-evoked flux was comparable between the genotypes (Figures 6B and 6C). Exposing sensory neurons to a 200 nM dose of capsaicin for a defined 5 s duration showed that the decay of calcium flux is accelerated in *SNS-Ubc9*$^{-/-}$ mice compared with Ubc9$^{fl/fl}$ mice (Figure 6D). In electrophysiological analyses of capsaicin-evoked currents, although the overall current density was comparable across the genotypes (Figures 6E and 6F), the deactivation time of TRPV1 currents was significantly lower in sensory neurons of *SNS-Ubc9*$^{-/-}$ mice compared with Ubc9$^{fl/fl}$ mice (Figures 6E and 6F). Thus, native TRPV1 channels in mouse DRGs are functionally impaired, although not completely abrogated, in sensory neurons upon loss of SUMOylation.

Analyses of TRPV1 function at the organismal scale corroborated our results from individual sensory neurons. Nocifensive responses to intraplantar paw injection of capsaicin, such as paw flicking, lifting, or licking, were strongly diminished in *SNS-Ubc9*$^{-/-}$ mice compared with Ubc9$^{fl/fl}$ mice (Figure 6G; 78% ± 4% decrease in specific TRPV1-mediated behavioral response). This did not result from decreased targeting of TRPV1 to nociceptive axons of *SNS-Ubc9*$^{-/-}$ mice, as measured by TRPV1 immunoprecipitation from distal sciatic nerve biopsies (Figure 6H).

To study the relation between TRPV1 function and diabetes-induced metabolic imbalance, we tested the effect of an increased lactate:pyruvate ratio on capsaicin-evoked calcium transients in cultured sensory neurons and observed that acutely exposing (30 min) mouse sensory neurons to lactate strongly reduced the proportion of neurons responding to capsaicin, although KCl-induced calcium transients were normal (Figure 6I). Similar results were obtained with methylglyoxal, another by-product of harmful metabolic pathways in diabetes, consistent with a previous study (Bierhaus et al., 2012; Figure 6I).

Generation and Analysis of Transgenic Mice Expressing SUMOylation-Deficient TRPV1 in Sensory Neurons

One caveat of deriving conclusions regarding alterations in TRPV1 function from *SNS-Ubc9*$^{-/-}$ mice is that an overall

Figure 5. Identification and Functional Validation of the Transient Receptor Potential V1 (TRPV1) Cation Channel as a Target of SUMOylation

(A) IP of native mouse TRPV1 (mTRPV1) in DRG neurons by anti-TRPV1 antibody (top blot) or anti-SUMO1 antibody (bottom blot), with anti-GFP IgG serving as a negative control.

(B and C) IP and IB on HEK cells co-expressing GFP and hemagglutinin (HA)-tagged rat TRPV1 (rTRPV1) in the wild-type (WT) form or the indicated mutants of potentially SUMOylated lysines (B) or their surrounding amino acids (leucine or glutamine) in the SUMOylation motif in rTRPV1 (C). IP was performed against the HA tag or against biotin following biotinylation rTRPV1 expressed at the cell surface.

(D) *In vitro* SUMOylation assay performed on purified HA-tagged rTRPV1 (1–363 amino acids).

(E) Change in proportion of SUMOylated rTRPV1 in the presence or absence of SENP1.

(F and G) Fura2-based imaging of calcium flux through WT or mutant rTRPV1 expressed in HEK cells upon exposure to the specific TRPV1 agonist capsaicin (1 μM). Shown are typical traces from multiple cells from one experiment (F) and quantitative summary from at least 30 cells/treatment/experiment and at least 4 independent such experiments (G) in the form of peak calcium or integral of the entire curve (AUC, area under the curve).

(H) Analysis of current density through rTRPV1 evoked by capsaicin application (1 mM) to Chinese hamster ovary (CHO) cells expressing WT or mutant TRPV1, using GFP expression as a negative control; N = 6 cells /treatment/experiment and at least 3 independent experiments. *$p < 0.05$ compared with WT rTRPV1; ANOVA of random measures followed by post hoc Kruskal-Wallis test.

In (B)–(E), arrows and arrowheads indicate the SUMOylated and un-SUMOylated forms of TRPV1, respectively, with tubulin as a loading control. Data represent mean ± SEM.

Please cite this article in press as: Agarwal et al., SUMOylation of Enzymes and Ion Channels in Sensory Neurons Protects against Metabolic Dysfunction, Neuropathy, and Sensory Loss in Diabetes, Neuron (2020), https://doi.org/10.1016/j.neuron.2020.06.037

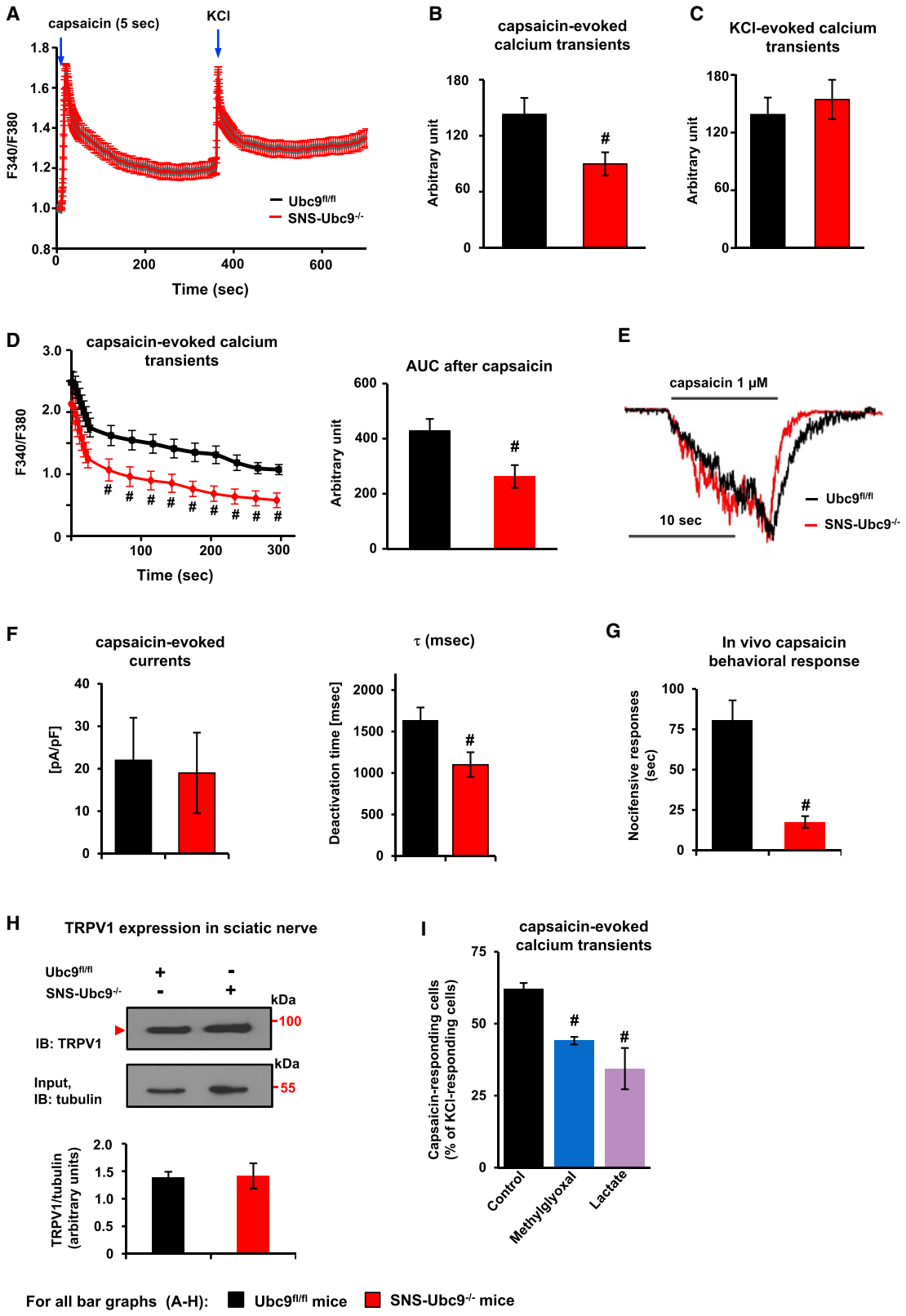

(legend on next page)

change in excitability of sensory neurons caused by de-SUMOylation of a number of other ion channels and proteins may also contribute to the *in vivo* phenotype we observed in response to capsaicin injections. Therefore, to elucidate the specific contribution of de-SUMOylated TRPV1 *in vivo*, we generated transgenic mice expressing HA-tagged wild-type mTRPV1 (SNS-mTRPV1^{WT}) or HA-tagged de-SUMOylated mTRPV1 (SNS-mTRPV1^{K325A}) in a sensory-neuron-specific manner (Figure 7A; Figure S4). In both cases, co-immunofluorescence analyses showed that the large majority (more than 80%) of nociceptors and only a small proportion of NF200-positive large-diameter neurons expressed TRPV1, as expected from the expression pattern of the $Na_v1.8$ bacterial artificial chromosome (Agarwal et al., 2004; Figures 7B and 7C; the negative control for anti-HA immunostaining is shown in Figure S4D).

Analysis of TRPV1 function via imaging of capsaicin-evoked calcium transients in these mice revealed that, in comparison with WT TRPV1, sensory neurons expressing de-SUMOylated mTRPV1 in the *TRPV1*$^{-/-}$ background showed strongly reduced responsivity to capsaicin, although responsivity to KCl was normal (see typical examples of traces in the top panel and quantitative summary in the bottom panel of Figure 7E). *In vivo* behavioral nocifensive responses to intraplantar capsaicin were significantly lower in magnitude in SNS-mTRPV1^{K325A} mice compared with SNS-mTRPV1^{wt} mice (Figure 7D). Moreover, following STZ injection, SNS-mTRPV1^{K325A} mice failed to develop thermal hyperalgesia over early (5–7 weeks) phases of DPN and showed a highly accelerated course of development of diabetic thermal hypoalgesia (Figure 7F, left panel), whereas mechanical hypersensitivity developed normally (Figure 7F, right panel). Analysis of paw intra-epidermal fiber density by immunostaining for PGP9.5 (Figure 7G) or CGRP (Figure S4E) up to 24 weeks post-STZ revealed a similar magnitude and time course of nerve fiber retraction across genotypes. Thus, altered TRPV1 function, not changes in peripheral nerve fiber density, account for the difference in behavioral sensitivity upon loss of TRPV1 SUMOylation *in vivo*. Taken together, all of the *ex vivo* and *in vivo* analyses described above indicate that SUMOylation is important for the functionality of TRPV1.

Diabetes Regulates SUMOylation of TRPV1 in Mouse Sensory Neurons

Because late stages of diabetes are characterized by sensory loss and hypoalgesia, we hypothesized that hypofunction of TRPV1 in DPN may be linked to a change in its SUMOylation status. Starting with equivalent quantities of nerve tissues, we immunoprecipitated SUMOylated proteins from sciatic nerves of mice 14 weeks post-STZ or control mice and observed that the proportion of SUMOylated TRPV1 was reduced in peripheral nerves of diabetic mice compared with the non-diabetic controls (Figure 7H; normalized to PGP9.5 to rule out artifacts because of potential loss of nerves).

Alterations in SUMOylation of Human Metabolic Enzymes and Human TRPV1 in Sciatic Nerves of Diabetic Patients

With a view toward testing the translational significance of our preclinical analyses, we performed immunoprecipitation with an anti-SUMO1 antibody on sciatic nerve biopsies from diabetic patients undergoing leg amputation because of chronic DPN, using sciatic nerves from healthy human donors as a control (Figure 8A). We observed that the proportion of SUMOylated TRPV1, but not the total quantity of TRPV1, was reduced in patients with DPN (normalized to tubulin; examples from 2 diabetic patients and non-diabetic donors each are shown in the top panels of Figure 8A, and a quantitative summary from 5 patients and controls each is shown in the bottom panel). Similarly, diabetic patients showed a decrease in levels of SUMOylated TKTL-1 and SUMOylated GAPDH in sciatic nerves, whereas total TKTL-1 and GAPDH levels were unchanged (Figures 8B and 8C). In contrast, the proportion of SUMOylated citrate synthase was increased significantly in diabetic patients (Figure 8D).

DISCUSSION

This study uncovers a previously undescribed neuroprotective role of SUMOylation in DRG neurons against metabolic damage and sensory loss in diabetes via regulation of key bioenergetic enzymes and sensory ion channels. A major novel finding is that GAPDH, a central player in maintaining metabolic balance via glycolysis, is positively regulated in activity by SUMOylation. This constitutes a novel mechanism for sustaining glycolysis in sensory neurons that may help counterbalance negative modulatory influence, such as inhibition of GAPDH activity by superoxide-mediated poly(ADP)-ribosylation (Du et al., 2003; Kanwar and Kowluru, 2009), which diverts upstream glycolytic metabolites in pathways of hyperglycemic damage (Feldman et al., 2017; Giacco and Brownlee, 2010). Here we obtained *in vitro*

Figure 6. Functional Validation of SUMOylation of Native TRPV1 in Sensory Neurons via Calcium Imaging, Electrophysiology, and Behavioral Analyses in *SNS-Ubc9*$^{-/-}$ Mice

(A–C) Calcium signals evoked by capsaicin (200 nM) in acutely dissociated small-diameter DRG neurons of *SNS-Ubc9*$^{-/-}$ mice and control Ubc9$^{fl/fl}$ mice. Shown are average traces from 40 neurons/genotype from one experiment (A), the integral AUC of response curves across all tested neurons derived from 4 mice/genotype (B), and responses of the same neurons to KCl (50 mM, C).

(D) Analysis of the kinetics of the decrease in capsaicin-evoked calcium flux following a brief (5 s) application of capsaicin (200 nM) followed by washout, shown as average traces from 40 neurons/genotype from one experiment (left) and AUC across all tested neurons derived from 4 mice/genotype (right).

(E and F) Patch-clamp analysis of currents evoked by capsaicin (1 μM) in DRG somata, showing the average current density and time constant of current deactivation current (τ); N = 11 neurons/genotype.

(G) Quantitative summary of *in vivo* nocifensive responses evoked by hindpaw intraplantar injection of capsaicin (0.06%, 20 μL).

(H) Typical example (top panel) and quantitative analysis of TRPV1 expression in the distal sciatic nerve via IB (normalized to tubulin, n = 3 mice/genotype).

(I) Calcium imaging on WT DRG neurons in response to 5-s application of capsaicin (500 nM) or KCl (50 mM); neurons were preincubated with methylglyoxal (100 μM) or lactate (3 mM) for 30 min.

#$p < 0.05$ compared across genotypes for the same treatment; ANOVA of random measures followed by post hoc Tukey's test. Data represent mean ± SEM.

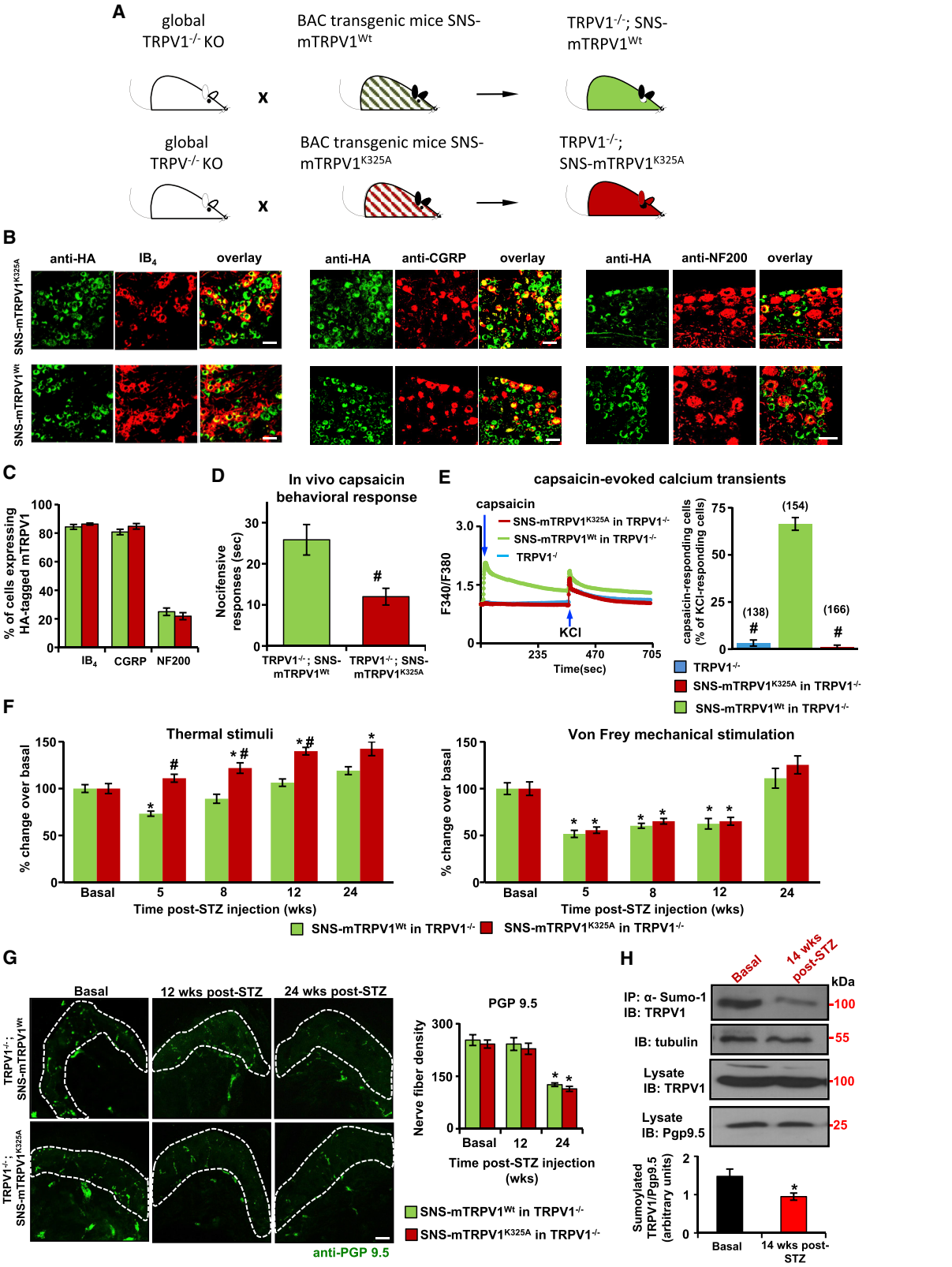

(legend on next page)

as well as *in vivo* evidence that diabetes-induced impairment of GAPDH SUMOylation underlies reduced activity of GAPDH in sensory neurons. This may have broad functional relevance for neurodegeneration, given the emerging role of GAPDH as a common target for diverse neurodegenerative disorders (Mazzola and Sirover, 2002).

Second, our data showed that four important catalytic enzymes from the Krebs cycle as well as pyruvate dehydrogenase are subject to SUMOylation in sensory neurons and that diabetes-induced suppression of the Krebs cycle in sensory neurons is further exacerbated in the absence of SUMOylation, promoting depletion of the energy supply. Notably, additional putative SUMOylation targets in sensory neurons also include other enzymes' important roles in mitochondrial function and energy metabolism. Because long axons of peripheral sensory neurons are particularly susceptible to energy demands because of the necessity of axonal transport over large distances, dysregulation of SUMOylation in pathways of carbohydrate metabolism and mitochondrial function in peripheral neurons could particularly predispose them to a bioenergetic crisis, serving as a primary trigger for neuropathic damage.

In addition to depleting the energy supply, we noted that loss of SUMOylation also promotes pathways leading to tissue damage (e.g., via a progressive increase in the lactate:pyruvate ratio in sensory neurons over the course of diabetic neuropathy, which is indicative of impairment of cellular respiration and malfunction of the TCA cycle in mitochondrial cytopathies; Nishikawa et al., 2000; Poggi-Travert et al., 1996), consistent with our finding that lactate dehydrogenase is a SUMOylation target in sensory neurons. Moreover, given our finding that lactate impairs TRPV1 channel function in sensory neurons, chronic accumulation of lactate would promote functional sensory loss associated with DPN. We also observed that impairment of SUMOylation in sensory neurons leads to accumulation of sorbitol, which is generated upon increased glucose flux through the harmful aldose reductase polyol pathway (Nishikawa et al., 2000;Gonçalves et al., 2017). Furthermore, we found that SUMOylation regulates the activity of the enzyme transketolase, which connects the pentose phosphate pathway to glycolysis and feeds excess sugar phosphates back into the main carbohydrate metabolic pathways and is necessary for production of reduced form of nicotinamide adenine dinucleotide phosphate (NADPH) (Zhao and Zhong, 2009). Because transketolase was found to be de-SUMOylated in peripheral nerves of diabetic patients and mice, this represents a mechanism for accumulation of harmful sugar phosphates intermediates as well as suppression of the cellular antioxidant response, exacerbating oxidative stress-induced pathology. Finally, we found that SUMOylation regulates the activity of the enzyme ALDH3A1, which metabolizes highly reactive aldehydes released during oxidative cellular damage and is known to protect the cornea from damage inflicted by ROS, UV light, and other oxidative stressors (Pappa et al., 2003). Thus, diabetes-induced de-SUMOylation is expected to exacerbate cellular damage via reactive aldehydes. Finally, we note that several well-studied heat shock proteins (HSPs), which have antioxidant functions, are critically involved in the cellular response to stress by acting as chaperones (Preuss et al., 2015), are putative SUMOylation targets in sensory neurons. In summary, de-SUMOylation over the course of diabetes elicits metabolic dysfunction, respiratory distress, and oxidative stress in sensory neurons, contributing to nerve damage and functional sensory loss in DPN.

Moreover, the results of our *in silico* screen suggest that SUMOylation may also directly alter nociceptive sensitivity in diabetes via SUMO binding in diverse ion channels mediating sensory transduction and transmission. Importantly, we uncovered an important role of SUMOylation in TRPV1 function, a channel required for nociceptive sensitization in a number of pathological pain conditions (Tominaga et al., 1998; Caterina and Julius 2001; Patapoutian et al., 2009). Comprehensive biochemical and mutational analyses identified residue K324 as the SUMOylation site, which lies in the N terminus in close proximity to Ankyrin repeat domains (ARDs). Recent structural elucidation of the TRPV1 channel not only confirms the ARD to be an important locus for channel modulation in the context of ATP binding and Ca^{2+}-calmodulin-dependent desensitization but also suggests that it serves as a surface for interaction with cellular factors or interactions between cytoplasmic domains involved in subunit organization (Liao et al., 2013). Consistent with the above, when we mutated the SUMOylation site and exclusively expressed de-SUMOylated mutant TRPV1, we observed complete loss of channel function in *in vitro* calcium imaging and patch-clamp analyses, although membrane localization was normal. The *in vivo* significance of these data was highlighted by transgenic mice expressing SUMOylation-deficient TRPV1, which showed lack of capsaicin transients in DRG sensory neurons and abrogation of TRPV1-mediated thermal hyperalgesia in early stages of diabetes and acceleration of

Figure 7. Generation and *In Vivo* Analysis of Genetically Modified Mice Specifically Lacking SUMOylated mTRPV1 in Sensory Neurons

(A) strategy for expression of WT HA-tagged mTRPV1 (*TRPV1*$^{-/-}$; SNS-mTRPV1^{WT}) or a de-SUMOylated HA-tagged mutant of mTRPV1 (*TRPV1*$^{-/-}$; SNS-mTRPV1^{K325A}) in mice globally lacking TRPV1 (*TRPV1*$^{-/-}$).

(B and C) Typical examples (B) and quantitative summary (C) of expression of TRPV1 in DRG neuron types labeled immunohistochemically for binding to IB_4 (non-peptidergic nociceptors), CGRP (peptidergic nociceptors), or NF200 (large-diameter neurons).

(D) *In vivo* nocifensive responses evoked by intraplantar hindpaw injection of capsaicin (0.06%, 20 μL).

(E) Calcium signals in response to 5-s application of capsaicin (500 nM) or KCl (50 mM) in acutely dissociated DRG neurons.

(F) Percent change in thermal latency or in response thresholds over baseline values 5, 8, 14, and 24 weeks post-STZ; N = 12 mice/genotype.

(G) Representative examples and quantitative summary of anti-PGP9.5-immunoreactive nerve endings in the plantar epidermis (dashed lines) in naive mice or and over 24 weeks post-STZ.

(H) Example blot (top panel) and quantitative comparative analysis (bottom panel) of SUMOylated TRPV1 in sciatic nerves of WT mice 14 weeks post-STZ treatment compared with age-matched non-diabetic controls (anti-PGP9.5, protein input control).

#$p < 0.05$ compared across genotypes for the same treatment; *$p < 0.05$ compared with basal. Student's t test (D and G) or ANOVA of random measures (C) or repeated measures (F and G), followed by post hoc Tukey's test. Scale bars represent 30 μm in (B) and 25 μm in (G). Data represent mean ± SEM.

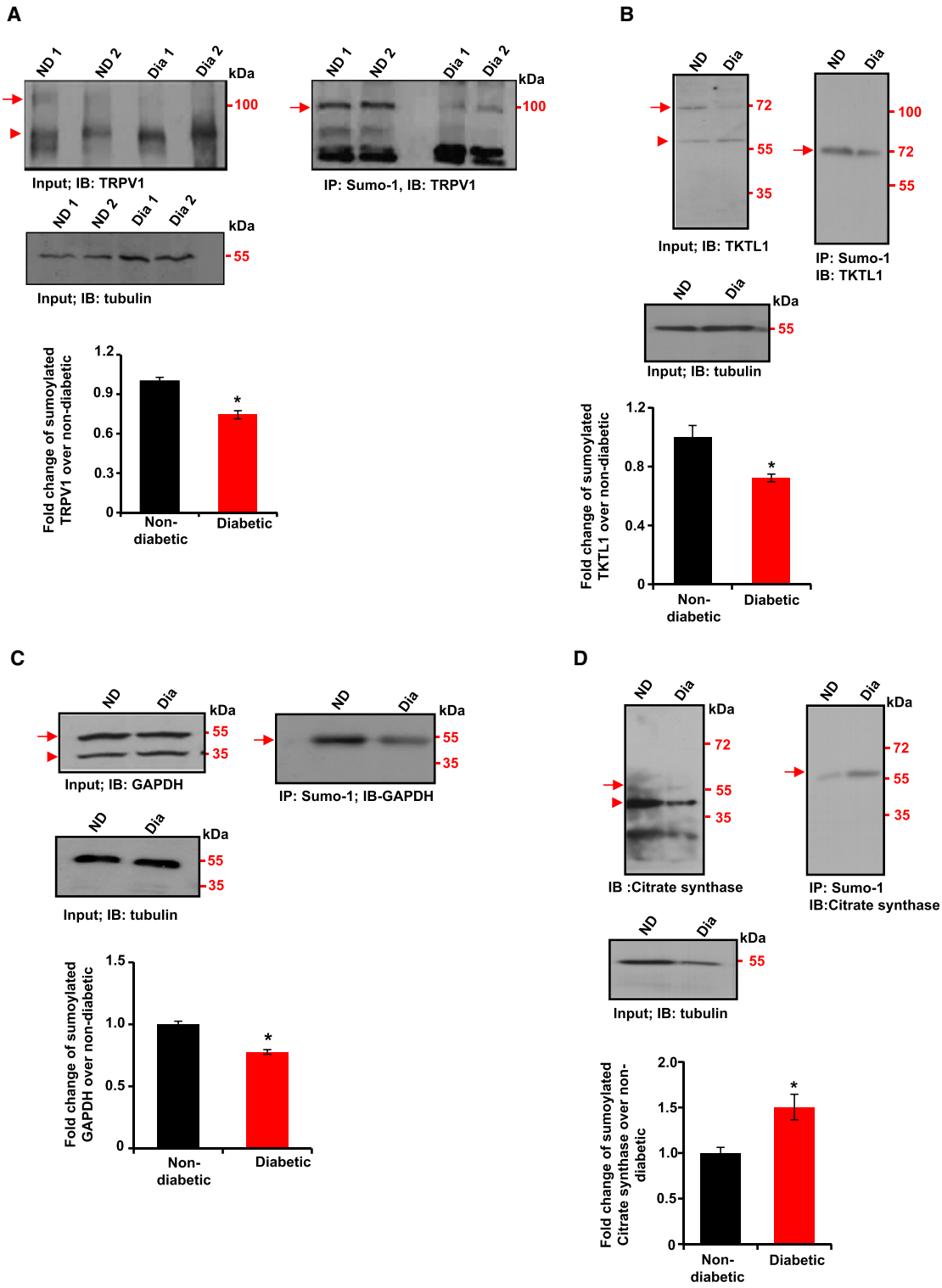

Figure 8. Expression and IP of SUMOylation Targets in Human Sciatic Nerve Tissue from Non-diabetic Donors (ND) and Diabetic Patients (Dia)

(A–D) Levels of anti-SUMO1 immunoprecipitated forms of TRPV1 (A), TKTL1 (B), GAPDH (C), and citrate synthase (D), normalized to tubulin expression within each specimen. Arrows and arrowheads indicate SUMOylated and un-SUMOylated proteins, respectively. N = 5 each for non-diabetic and diabetic samples. *$p < 0.05$ between diabetic and non-diabetic human nerve tissue, Student's t test. Data represent mean + SEM.

late-onset thermal hypoalgesia, which has been linked to reduced TRPV1 function in late stages of DPN (Lee et al., 2015; Pabbidi et al., 2008; Hong and Wiley, 2005).

However, complete loss of TRPV1 function, as expected from data from the heterologous or transgenic situation with homomeric mutant TRPV1 expression, was not observed in sensory neuron somata of *SNS-Ubc9*$^{-/-}$ mice. One cannot fully rule out compensatory changes in *SNS-Ubc9*$^{-/-}$ mice (e.g., induced by perinatal deletion of Ubc9); orthogonal, secondary effects on TRPV1 because SUMOylation of numerous proteins is affected; or partial restoration of TRPV1 function by other compensatory post-translational modifications (e.g., acetylation, which has been shown to compete with SUMOylation in the case of several proteins; Van Rechem et al., 2010; de la Vega et al., 2012). Alternatively, mutating K324 may affect TRPV1 channel function independent of SUMOylation (e.g., via structural alterations in the ARD domain), which is, however, mitigated by our observations of the lack of effects of other mutations in this region. Thus, a more detailed analysis of TRPV1 regulation by SUMOylation is warranted in the future, and deriving the crystal structure of TRPV1 SUMOylation mutants may shed more light on the nature of modulation. Nevertheless, two observations in *SNS-Ubc9*$^{-/-}$ mice also strongly support the importance of SUMOylation in TRPV1 regulation. First, *SNS-Ubc9*$^{-/-}$ mice demonstrated a stronger phenotype at the level of peripheral TRPV1 function (e.g., nocifensive responses to capsaicin or diabetes-associated changes in heat sensitivity) compared with analyses of somata, suggesting potential differences in configuration and regulation of TRPV1 channels at somata versus axon terminals. Second, they demonstrated a major reduction in calcium influx under conditions where TRPV1 was activated repeatedly, suggesting a particularly significant effect in states associated with persistent recruitment of TRPV1 by algogens, which is true for chronic pain, including DPN. Our finding that the SUMOylated fraction of native TRPV1 is significantly depleted in nerves of diabetic mice and patients would indicate that the functional effect of de-SUMOylation of TRPV1 is increased further in DPN. Finally, because TRPV1 is linked to diabetes at multiple levels, including pancreatic function and insulin release, appetite control and energy expenditure or thermogenesis (Wang et al., 2012), modulation of TRPV1 function by SUMOylation outside of sensory neurons may even alter the course of diabetes.

We therefore conclude that SUMOylation is an important mechanism for endogenous protection from metabolic damage in sensory neurons in DPN, and modulation of the SUMOylation status of specific molecular targets may yield new strategies for treatment and reversal of DPN, such as the recently developed small-molecule SUMO activators (Krajnak and Dahl, 2018).

STAR★METHODS

Detailed methods are provided in the online version of this paper and include the following:

- KEY RESOURCES TABLE
- RESOURCE AVAILABILITY
  - Lead Contact
  - Materials Availability
  - Data and Code Availability
- EPERIMENTAL MODEL AND SUBJECT DETAILS
  - Animals
  - Cell Culture and Transfections
  - Primary DRG cell cultures
- METHOD DETAILS
  - Transgenic mouse lines
  - Generation of BAC transgenic mice
  - Mouse tissue preparation
  - Mouse model of type 1 diabetes
  - Behavioral measurements
  - Plasmids and purified protein
  - Antibodies
  - Cell surface protein expression
  - Immunoprecipitation and western blot analysis
  - *In vitro* SUMOylation assay
  - Site-directed mutagenesis
  - Calcium imaging
  - Immunohistochemistry
  - Activity assays
  - GAPDH activity assay
  - Citrate synthase activity assay
  - Aldehyde Dehydrogenase (ALDH) activity assay
  - Transketolase activity assay
  - Mass-spectrometry analysis (LC/MS-MS)
  - Metabolite analysis by GC/MS
  - *In silico* prediction of SUMOylation sites
  - Human tissue
- QUANTIFICATION AND STATISTICAL ANALYSIS
- ADDITIONAL RESOURCES

SUPPLEMENTAL INFORMATION

Supplemental Information can be found online at https://doi.org/10.1016/j.neuron.2020.06.037.

ACKNOWLEDGMENTS

The authors are grateful to D. Baumgartl-Ahlert for technical assistance. We acknowledge support from the Interdisciplinary Neurobehavioral Core (INBC), the Proteomics facility, and the Metabolomics facility at Heidelberg University. We acknowledge support from the tissue bank of the National Centre for Tumour Diseases (NCT, Heidelberg, Germany) in accordance with the regulations of the tissue bank and approval from the ethics committee of Heidelberg University (Ethic Votes 206/2005 and 207/2005). This work was supported by Deutsche Forschungsgemeinschaft grants SFB1118 (project B06) (to N.A. and R.K.), SFB1118 (projects A04, S02, and S01) (to P.P.N., E.H., and T.F.), SFB1158 (project A01) (to S.G.L.), and SFB1158 (project A03) (to P.P.N.). R.K. is a member of the Molecular Medicine Partnership Unit, Heidelberg and a principal investigator in the Excellence Cluster "CellNetworks" of Heidelberg University.

AUTHOR CONTRIBUTIONS

N.A., D.R.R., C.N., F.J.T., M.M., D.O., F.F., P.G., A.A., and K.K.B. performed the experiments and/or analyzed data. R.K. primarily designed and supervised the study. N.A. and R.K. designed and supervised the experiments. A.A., A.D., and E.H. provided materials. A.D., T.F., P.P.N., G.R.L., and S.G.L. provided conceptual input regarding the experiments and feedback regarding the manuscript. R.K. and N.A. primarily wrote the manuscript.

DECLARATION OF INTERESTS

The authors declare no competing interests.

Received: November 23, 2019
Revised: April 20, 2020
Accepted: June 26, 2020
Published: July 30, 2020

REFERENCES

Agarwal, N., Offermanns, S., and Kuner, R. (2004). Conditional gene deletion in primary nociceptive neurons of trigeminal ganglia and dorsal root ganglia. Genesis *38*, 122–129.

Agarwal, N., Helmstädter, J., Rojas, D.R., Bali, K.K., Gangadharan, V., and Kuner, R. (2018). Evoked hypoalgesia is accompanied by tonic pain and immune cell infiltration in the dorsal root ganglia at late stages of diabetic neuropathy in mice. Mol. Pain *14*, 1744806918817975.

Becker, J., Barysch, S.V., Karaca, S., Dittner, C., Hsiao, H.H., Berriel Diaz, M., Herzig, S., Urlaub, H., and Melchior, F. (2013). Detecting endogenous SUMO targets in mammalian cells and tissues. Nat. Struct. Mol. Biol. *20*, 525–531.

Benson, M.D., Li, Q.J., Kieckhafer, K., Dudek, D., Whorton, M.R., Sunahara, R.K., Iñiguez-Lluhí, J.A., and Martens, J.R. (2007). SUMO modification regulates inactivation of the voltage-gated potassium channel Kv1.5. Proc. Natl. Acad. Sci. USA *104*, 1805–1810.

Berkefeld, H., Sailer, C.A., Bildl, W., Rohde, V., Thumfart, J.O., Eble, S., Klugbauer, N., Reisinger, E., Bischofberger, J., Oliver, D., et al. (2006). BKCa-Cav channel complexes mediate rapid and localized Ca2+-activated K+ signaling. Science *314*, 615–620.

Bernier-Villamor, V., Sampson, D.A., Matunis, M.J., and Lima, C.D. (2002). Structural basis for E2-mediated SUMO conjugation revealed by a complex between ubiquitin-conjugating enzyme Ubc9 and RanGAP1. Cell *108*, 345–356.

Bierhaus, A., Fleming, T., Stoyanov, S., Leffler, A., Babes, A., Neacsu, C., Sauer, S.K., Eberhardt, M., Schnölzer, M., Lasitschka, F., et al. (2012). Methylglyoxal modification of Nav1.8 facilitates nociceptive neuron firing and causes hyperalgesia in diabetic neuropathy. Nat. Med. *18*, 926–933.

Boulton, A.J., Vileikyte, L., Ragnarson-Tennvall, G., and Apelqvist, J. (2005). The global burden of diabetic foot disease. Lancet *366*, 1719–1724.

Caterina, M.J., and Julius, D. (2001). The vanilloid receptor: a molecular gateway to the pain pathway. Annu. Rev. Neurosci. *24*, 487–517.

Chamberlain, B.R., Buttery, J.E., and Pannall, P.R. (1996). A stable reagent mixture for the whole blood transketolase assay. Ann. Clin. Biochem. *33*, 352–354.

Chua, J.P., Reddy, S.L., Yu, Z., Giorgetti, E., Montie, H.L., Mukherjee, S., Higgins, J., McEachin, R.C., Robins, D.M., Merry, D.E., et al. (2015). Disrupting SUMOylation enhances transcriptional function and ameliorates polyglutamine androgen receptor-mediated disease. J. Clin. Invest. *125*, 831–845.

Dai, X.Q., Plummer, G., Casimir, M., Kang, Y., Hajmrle, C., Gaisano, H.Y., Manning Fox, J.E., and MacDonald, P.E. (2011). SUMOylation regulates insulin exocytosis downstream of secretory granule docking in rodents and humans. Diabetes *60*, 838–847.

de la Vega, L., Grishina, I., Moreno, R., Krüger, M., Braun, T., and Schmitz, M.L. (2012). A redox-regulated SUMO/acetylation switch of HIPK2 controls the survival threshold to oxidative stress. Mol. Cell *46*, 472–483.

Du, X., Matsumura, T., Edelstein, D., Rossetti, L., Zsengellér, Z., Szabó, C., and Brownlee, M. (2003). Inhibition of GAPDH activity by poly(ADP-ribose) polymerase activates three major pathways of hyperglycemic damage in endothelial cells. J. Clin. Invest. *112*, 1049–1057.

Duh, E.J., Sun, J.K., and Stitt, A.W. (2017). Diabetic retinopathy: current understanding, mechanisms, and treatment strategies. JCI Insight *2*, 14.

Feldman, E.L., Nave, K.A., Jensen, T.S., and Bennett, D.L.H. (2017). New Horizons in Diabetic Neuropathy: Mechanisms, Bioenergetics, and Pain. Neuron *93*, 1296–1313.

Forbes, J.M., and Cooper, M.E. (2013). Mechanisms of diabetic complications. Physiol. Rev. *93*, 137–188.

Geiss-Friedlander, R., and Melchior, F. (2007). Concepts in sumoylation: a decade on. Nat. Rev. Mol. Cell Biol. *8*, 947–956.

Giacco, F., and Brownlee, M. (2010). Oxidative stress and diabetic complications. Circ. Res. *107*, 1058–1070.

Gonçalves, N.P., Vægter, C.B., Andersen, H., Østergaard, L., Calcutt, N.A., and Jensen, T.S. (2017). Schwann cell interactions with axons and microvessels in diabetic neuropathy. Nat. Rev. Neurol. *13*, 135–147.

Gram, D.X., Holst, J.J., and Szallasi, A. (2017). TRPV1: A Potential Therapeutic Target in Type 2 Diabetes and Comorbidities? Trends Mol. Med. *23*, 1002–1013.

Hong, S., and Wiley, J.W. (2005). Early painful diabetic neuropathy is associated with differential changes in the expression and function of vanilloid receptor 1. J. Biol. Chem. *280*, 618–627.

Johnson, E.S. (2004). Protein modification by SUMO. Annu. Rev. Biochem. *73*, 355–382.

Kahya, M.C., Nazıroğlu, M., and Övey, İ.S. (2017). Modulation of Diabetes-Induced Oxidative Stress, Apoptosis, and Ca^{2+} Entry Through TRPM2 and TRPV1 Channels in Dorsal Root Ganglion and Hippocampus of Diabetic Rats by Melatonin and Selenium. Mol. Neurobiol. *54*, 2345–2360.

Kanwar, M., and Kowluru, R.A. (2009). Role of glyceraldehyde 3-phosphate dehydrogenase in the development and progression of diabetic retinopathy. Diabetes *58*, 227–234.

Koulmanda, M., Qipo, A., Chebrolu, S., O'Neil, J., Auchincloss, H., and Smith, R.N. (2003). The effect of low versus high dose of streptozotocin in cynomolgus monkeys (Macaca fascilularis). Am. J. Transplant. *3*, 267–272.

Krajnak, K., and Dahl, R. (2018). Small molecule SUMOylation activators are novel neuroprotective agents. Bioorg. Med. Chem. Lett. *28*, 405–409.

Lee, E., Jung, D.Y., Kim, J.H., Patel, P.R., Hu, X., Lee, Y., Azuma, Y., Wang, H.F., Tsitsilianos, N., Shafiq, U., et al. (2015). Transient receptor potential vanilloid type-1 channel regulates diet-induced obesity, insulin resistance, and leptin resistance. FASEB J. *29*, 3182–3192.

Li, M., Guo, D., Isales, C.M., Eizirik, D.L., Atkinson, M., She, J.X., and Wang, C.Y. (2005). SUMO wrestling with type 1 diabetes. J. Mol. Med. (Berl.) *83*, 504–513.

Liao, M., Cao, E., Julius, D., and Cheng, Y. (2013). Structure of the TRPV1 ion channel determined by electron cryo-microscopy. Nature *504*, 107–112.

Lim, A.K.h. (2014). Diabetic nephropathy - complications and treatment. Int. J. Nephrol. Renovasc. Dis. *7*, 361–381.

Luo, C., Gangadharan, V., Bali, K.K., Xie, R.G., Agarwal, N., Kurejova, M., Tappe-Theodor, A., Tegeder, I., Feil, S., Lewin, G., et al. (2012). Presynaptically localized cyclic GMP-dependent protein kinase 1 is a key determinant of spinal synaptic potentiation and pain hypersensitivity. PLoS Biol. *10*, e1001283.

Madsen-Bouterse, S., Mohammad, G., and Kowluru, R.A. (2010). Glyceraldehyde-3-phosphate dehydrogenase in retinal microvasculature: implications for the development and progression of diabetic retinopathy. Invest. Ophthalmol. Vis. Sci. *51*, 1765–1772.

Martin, S., Nishimune, A., Mellor, J.R., and Henley, J.M. (2007). SUMOylation regulates kainate-receptor-mediated synaptic transmission. Nature *447*, 321–325.

Mazzola, J.L., and Sirover, M.A. (2002). Alteration of intracellular structure and function of glyceraldehyde-3-phosphate dehydrogenase: a common phenotype of neurodegenerative disorders? Neurotoxicology *23*, 603–609.

McLaughlin, R.J., Spindler, M.P., van Lummel, M., and Roep, B.O. (2016). Where, How, and When: Positioning Posttranslational Modification Within Type 1 Diabetes Pathogenesis. Curr. Diab. Rep. *16*, 63.

Nacerddine, K., Lehembre, F., Bhaumik, M., Artus, J., Cohen-Tannoudji, M., Babinet, C., Pandolfi, P.P., and Dejean, A. (2005). The SUMO pathway is essential for nuclear integrity and chromosome segregation in mice. Dev. Cell *9*, 769–779.

Nawroth, P.P., Bendszus, M., Pham, M., Jende, J., Heiland, S., Ries, S., Schumann, C., Schmelz, M., Schuh-Hofer, S., Treede, R.D., et al. (2017). The quest for more research on painful diabetic neuropathy. Neuroscience *387*, 28–37.

Nishikawa, T., Edelstein, D., Du, X.L., Yamagishi, S., Matsumura, T., Kaneda, Y., Yorek, M.A., Beebe, D., Oates, P.J., Hammes, H.P., et al. (2000). Normalizing mitochondrial superoxide production blocks three pathways of hyperglycaemic damage. Nature *404*, 787–790.

Njoo, C., Agarwal, N., Lutz, B., and Kuner, R. (2015). The Cannabinoid Receptor CB1 Interacts with the WAVE1 Complex and Plays a Role in Actin Dynamics and Structural Plasticity in Neurons. PLoS Biol. *13*, e1002286.

Pabbidi, R.M., Yu, S.Q., Peng, S., Khardori, R., Pauza, M.E., and Premkumar, L.S. (2008). Influence of TRPV1 on diabetes-induced alterations in thermal pain sensitivity. Mol. Pain *4*, 9.

Pappa, A., Estey, T., Manzer, R., Brown, D., and Vasiliou, V. (2003). Human aldehyde dehydrogenase 3A1 (ALDH3A1): biochemical characterization and immunohistochemical localization in the cornea. Biochem. J. *376*, 615–623.

Patapoutian, A., Tate, S., and Woolf, C.J. (2009). Transient receptor potential channels: targeting pain at the source. Nat. Rev. Drug Discov. *8*, 55–68.

Poggi-Travert, F., Martin, D., Billette de Villemeur, T., Bonnefont, J.P., Vassault, A., Rabier, D., Charpentier, C., Kamoun, P., Munnich, A., and Saudubray, J.M. (1996). Metabolic intermediates in lactic acidosis: compounds, samples and interpretation. J. Inherit. Metab. Dis. *19*, 478–488.

Preuss, K.D., Pfreundschuh, M., Weigert, M., Fadle, N., Regitz, E., and Kubuschok, B. (2015). Sumoylated HSP90 is a dominantly inherited plasma cell dyscrasias risk factor. J. Clin. Invest. *125*, 316–323.

Sacher, M., Pfander, B., and Jentsch, S. (2005). Identification of SUMO-protein conjugates. Methods Enzymol. *399*, 392–404.

Seeler, J.S., and Dejean, A. (2003). Nuclear and unclear functions of SUMO. Nat. Rev. Mol. Cell Biol. *4*, 690–699.

Silveirinha, V., Stephens, G.J., and Cimarosti, H. (2013). Molecular targets underlying SUMO-mediated neuroprotection in brain ischemia. J. Neurochem. *127*, 580–591.

Simonetti, M., Agarwal, N., Stösser, S., Bali, K.K., Karaulanov, E., Kamble, R., Pospisilova, B., Kurejova, M., Birchmeier, W., Niehrs, C., et al. (2014). Wnt-Fzd signaling sensitizes peripheral sensory neurons via distinct noncanonical pathways. Neuron *83*, 104–121.

Tesfaye, N., and Seaquist, E.R. (2004). Silent hypoglycemia presenting as dysesthesias. Diabetes Care *27*, 628–629.

Tominaga, M., Caterina, M.J., Malmberg, A.B., Rosen, T.A., Gilbert, H., Skinner, K., Raumann, B.E., Basbaum, A.I., and Julius, D. (1998). The cloned capsaicin receptor integrates multiple pain-producing stimuli. Neuron *21*, 531–543.

Van Rechem, C., Boulay, G., Pinte, S., Stankovic-Valentin, N., Guérardel, C., and Leprince, D. (2010). Differential regulation of HIC1 target genes by CtBP and NuRD, via an acetylation/SUMOylation switch, in quiescent versus proliferating cells. Mol. Cell. Biol. *30*, 4045–4059.

Vicuña, L., Strochlic, D.E., Latremoliere, A., Bali, K.K., Simonetti, M., Husainie, D., Prokosch, S., Riva, P., Griffin, R.S., Njoo, C., et al. (2015). The serine protease inhibitor SerpinA3N attenuates neuropathic pain by inhibiting T cell-derived leukocyte elastase. Nat. Med. *21*, 518–523.

Wang, P., Yan, Z., Zhong, J., Chen, J., Ni, Y., Li, L., Ma, L., Zhao, Z., Liu, D., and Zhu, Z. (2012). Transient receptor potential vanilloid 1 activation enhances gut glucagon-like peptide-1 secretion and improves glucose homeostasis. Diabetes *61*, 2155–2165.

Witty, J., Aguilar-Martinez, E., and Sharrocks, A.D. (2010). SENP1 participates in the dynamic regulation of Elk-1 SUMOylation. Biochem. J. *428*, 247–254.

Yagihashi, S., Mizukami, H., and Sugimoto, K. (2011). Mechanism of diabetic neuropathy: Where are we now and where to go? J. Diabetes Investig. *2*, 18–32.

Yang, P., Hu, S., Yang, F., Guan, X.Q., Wang, S.Q., Zhu, P., Xiong, F., Zhang, S., Xu, J., Yu, Q.L., and Wang, C.Y. (2014). Sumoylation modulates oxidative stress relevant to the viability and functionality of pancreatic beta cells. Am. J. Transl. Res. *6*, 353–360.

Yau, T.Y., Molina, O., and Courey, A.J. (2020). SUMOylation in development and neurodegeneration. Development *147*, 1–9.

Zhao, J., and Zhong, C.J. (2009). A review on research progress of transketolase. Neurosci. Bull. *25*, 94–99.

Zhao, Q., Xie, Y., Zheng, Y., Jiang, S., Liu, W., Mu, W., Liu, Z., Zhao, Y., Xue, Y., and Ren, J. (2014). GPS-SUMO: a tool for the prediction of sumoylation sites and SUMO-interaction motifs. Nucleic Acids Res. *42*, W325-30.

Zheng, H., Wu, J., Jin, Z., and Yan, L.J. (2016). Protein Modifications as Manifestations of Hyperglycemic Glucotoxicity in Diabetes and Its Complications. Biochem. Insights *9*, 1–9.

Please cite this article in press as: Agarwal et al., SUMOylation of Enzymes and Ion Channels in Sensory Neurons Protects against Metabolic Dysfunction, Neuropathy, and Sensory Loss in Diabetes, Neuron (2020), https://doi.org/10.1016/j.neuron.2020.06.037

STAR★METHODS

KEY RESOURCES TABLE

REAGENT or RESOURCE	SOURCE	IDENTIFIER
Antibodies		
Rat anti-HA	Roche	RRID: AB_390919
Rabbit anti-HA	Cell signaling	RRID: AB_10693385
Mouse anti-HA	Covance	RRID: AB_291259
Mouse anti-Sumo1	DSHB	RRID: AB_2198257
Mouse anti-GFP	DSHB	RRID: AB_2617419
Rabbit anti-GAPDH	Thermo Scientific	RRID: AB_568552
Rabbit anti-tubulin	Sigma Aldrich	RRID: AB_261659
Rabbit anti-TKTL1	Sigma Aldrich	RRID: AB_10665408
Rabbit anti-citrate synthase	Thermo Scientific	RRID: AB_2787810
Mouse anti-ALDH	Origene	RRID: AB_10774056
Rabbit anti-pgp9.5	Dako	RRID: AB_2622233
Rabbit anti-NF200	Sigma Aldrich	RRID: AB_477272
Biotinylated Griffonia simplicifolia Isolectin-B4 (IB4)	Vector lab	RRID: AB_2314661
Rabbit anti-FLAG	Sigma Aldrich	RRID: AB_2811010
Rabbit anti-CGRP	Immuno star	RRID: AB_572217
Goat anti-Ubc9	Santa Cruz	RRID: AB_2256740
Rabbit anti-GFP	Sigma Aldrich	RRID: AB_2750576
Donkey anti rabbit-Alexa Fluor 488	Invitrogen	RRID: AB_2762833
Donkey anti-rabbit-Alexa Fluor 594	Invitrogen	RRID: AB_2762827
Donkey anti-goat-Alexa Fluor 488	Invitrogen	RRID: AB_2762838
Streptavidin-Alexa Fluor 594	Invitrogen	RRID: AB_2315780
Anti-mouse-HRP	GE healthcare	RRID: AB_772210
Anti-rabbit-HRP	Sigma Aldrich	RRID: AB_772206
Anti-goat-HRP	Santa Cruz	RRID: AB_631728
Bacterial and Virus Strains		
One Shot MAX Efficiency DH5α-T1^R	ThermoFisher Scientific	Cat#12297016
NEB® 5-alpha Competent *E. coli*	New England Biolabs	Cat#C2987H
Biological Samples		
Human sciatic nerve materials	NCT Heidelberg	https://www.nct-heidelberg.de/
Chemicals, Peptides, and Recombinant Proteins		
Kanamycin sulfate	Sigma-Aldrich	Cat#B5264
Ampicillin	Sigma-Aldrich	Cat#A9393
Chloramphenicol	Sigma-Aldrich	Cat#C3175
Tetracycline hydrochloride	Sigma-Aldrich	Cat#T7660
N-Ethylmaleimide	Sigma-Aldrich	Cat#E3876
Streptozocin	Sigma-Aldrich	Cat#S0130
SENP1 catalytic domain	BostonBiochem	Cat#E-700
SENP2 catalytic domain	BostonBiochem	Cat#E-710
Purified GAPDH	ScienCell™	Cat#8148h
3X FLAG® Peptide	Sigma-Aldrich	Cat#4799
HA peptide	Sigma-Aldrich	Cat#11666975001

(*Continued on next page*)

Continued

REAGENT or RESOURCE	SOURCE	IDENTIFIER
Critical Commercial Assays		
Quick & Easy BAC Modification Kit	Genebridges	Cat#K001
QIAquick PCR Purification kit	QIAGEN	Cat#28104
QIAquick Gel Extraction kit	QIAGEN	Cat#28115
SUMOlink (*In vitro* SUMOylation kit)	Activmotif	Cat#40120
GeneArt™ Site-directed mutagenesis PLUS	ThermoFisher	Cat#A14604
GAPDH Assay	ScienCell™	Cat#8148
Aldehyde dehydrogenase activity assay	Sigma-Aldrich	Cat#MAK082
Citrate synthase activity assay	Sigma-Aldrich	Cat#MAK193
Experimental Models: Cell Lines		
HEK293	ATCC	CVCL_0045
Mouse DRG culture	This study	N/A
Experimental Models: Organisms/Strains		
C57BL/6J mice	Janvier, Europe	RRID:IMSR_JAX:000664
Ubc9$^{flox/flox}$ mice: Ube2i^{tm1Adej}		RRID:MGI:4430411
SNS-Cre mice: Tg(Scn10a-cre)1Rkun		MGI:3042874
TRPV1$^{-/-}$ mice: B6.129X1-Trpv1^{tm1Jul}		RRID:MGI:4418342
SNSUbc9$^{-/-}$: Tg(Scn10a-cre)1Rkun:Ube2i^{tm1Adej}	In this study	N/A
Oligonucleotides		
GAPDH-K59A forward GCAAATTCAACGGCACAG TCGCCGCCGAGAATG	In this study	N/A
GAPDH-K59R forward GCAAATTCAACGGCACAGT CCGGGCCGAGAATG	In this study	N/A
GAPDH-K59 reverse GACTGTGCCGTTGAATTTG CCGTGGGTGGAGTC	In this study	N/A
GAPDH-K257 forward CTGCCAAGTATGATGACAT CGCCAAGGTGGTGAA	In this study	N/A
GAPDH-K257 reverse GATGTCATCATACTTGGCA GGTTTCTCCAGGCGG	In this study	N/A
TRPV1-L323A forward GCCAAACTGCACCCGACG GCCAAGCTGGAGGAGCTCACCA	In this study	N/A
TRPV1-L323A reverse TGGTGAGCTCCTCCAGCTTG GCCGTCGGGTGCAGTTTGGC	In this study	N/A
TRPV1-K324R forward GCCAAACTGCACCCGACGC TGCGGCTGGAGGAGCTCACCA	In this study	N/A
TRPV1-K324R reverse TGGTGAGCTCCTCCAGCCGC AGCGTCGGGTGCAGTTTGGC	In this study	N/A
TRPV1-E326A forward GCACCCGACGCTGAAGCTG GCCGAGGAGCTCACCAACAAGAAG	In this study	N/A

(*Continued on next page*)

Please cite this article in press as: Agarwal et al., SUMOylation of Enzymes and Ion Channels in Sensory Neurons Protects against Metabolic Dysfunction, Neuropathy, and Sensory Loss in Diabetes, Neuron (2020), https://doi.org/10.1016/j.neuron.2020.06.037

Continued

REAGENT or RESOURCE	SOURCE	IDENTIFIER
TRPV1-E326 reverse CTTCTTGTTGGTGAGCTCGGCC AGCCGCAGCGTCGGGTGC	In this study	N/A
TRPV1-L325Y forward GCACCCGACGCTGAAGTAT GAGGAGCTCACCAACAAGAAG	In this study	N/A
TRPV1-L325Y reverse CTTCTTGTTGGTGAGCTCCTCA TACTTCAGCGTCGGGTGC	In this study	N/A
Recombinant DNA		
pIRES2-AcGFP1	Clontech	Cat#632435
Myc-DKK-tagged GAPDH in pCMV6-entry	Origene	Cat#MR204934
Senp1 mouse tagged in pCMV-Ac-GFP	Origene	Cat#MG209692
Software and Algorithms		
Graphpad Prism	Graphpad	https://www.graphpad.com/scientific-software/prism/
GPS-SUMO	Cuckoo	http://sumosp.biocuckoo.org/online.php
SUMOplot Analysis Program	OMICS_02437	N/A
ImageJ	Fiji	https://fiji.sc/
Other		
not applicable	not applicable	not applicable

RESOURCE AVAILABILITY

Lead Contact

Requests for further information and resources should be directed to the lead contact, Rohini Kuner at rohini.kuner@pharma.uni-heidelberg.de

Materials Availability

Mouse lines generated in this study are available upon request.

Data and Code Availability

The dataset supporting the current study are available from the lead contact upon request.

EPERIMENTAL MODEL AND SUBJECT DETAILS

Animals

All experiments were performed on an equal number of male and female animals. 8 wks-old wild-type C57BL6/j mice (RRID:IMSR_JAX:000664) were purchased from Janvier, Europe. All animals were housed in individually ventilated cages with stable environment maintained at 22 ± 1°C with a 12/12-hr light-dark cycle. Four animals were housed in individually ventilated cage-rack system (Techniplast, Italy). All animals had free access to water and food. All experimental procedures were approved by Animal Care and Ethics Committee (Regierungspräsidium), Karlsruhe, Germany. All attempts were made to follow the ARRIVE guidelines. The experimenters were blinded to the identity of mice being analyzed.

Cell Culture and Transfections

Human embryonic kidney 293 (HEK293) cells were maintained in 10% FBS in DMEM media according to routine protocols. 15 μg of plasmid were transfected using calcium chloride transfection protocol. The transfected cells were harvested after 48 hr. of transfection for further analysis.

Primary DRG cell cultures

DRG cell cultures were made from 6-8 wks old SNS-Ubc9$^{-/-}$ and Ubc9$^{fl/fl}$ mice. Mice were killed with CO_2 and DRG were extracted in ice-cold DMEM. The extracted DRGs were incubated in a digestive mixture of trypsin, collagenase, and DNase for 30 min at 37°C.

The cells were washed with DMEM media containing 10% FBS. The DRG cells were plated on poly L-lysine coated glass coverslip and cultured in complete DMEM media without growth factors for 24 hr. prior to calcium imaging.

METHOD DETAILS

Transgenic mouse lines

SNS-Cre mice (MGI:304274), which allow sensory neuron-specific gene deletion selectively in nociceptive and thermoreceptive neurons with a perinatal onset (Agarwal et al., 2004), were mated with mice carrying floxed alleles of the murine *Ubc9* gene (Ubc9$^{fl/fl}$ mice; RRID:MGI:4430411) (Nacerddine et al., 2005), a key E2 ligase that is critically required for SUMO conjugation to lysine's in target proteins (Seeler and Dejean, 2003). Homozygous mice carrying the floxed allele of the mouse *Ube2i*, which encodes ubiquitin-conjugating enzyme E28 (Ubc9), have been described previously in details (Ubc9$^{fl/fl}$) (Nacerddine et al., 2005). Ubc9$^{fl/fl}$ mice were crossed with SNS-Cre (Agarwal et al., 2004) mice to obtain SNS-Cre^{+}; Ubc9$^{fl/fl}$ mice (referred to as SNS-Ubc9$^{fl/fl}$ mice) and SNS-Cre^{-}; Ubc9$^{fl/fl}$ mice (control littermates). Mice were crossed into the C57BL6/j background for more than 8 generations. Only littermates were used in all behavioral experiments.

Generation of BAC transgenic mice

A cassette consisting of the either Hemagglutinin(HA)-tagged-mouse Transient Receptor Potential Vanilloid 1-wild-type {HA-mTRPV1(wt)} or HA-tagged mutant mouse Transient Receptor Potential Vanilloid 1 (K325A) {HA-mTRPV1(K325A)} followed by a β-actin polyA sequence and a module containing the β-lactamase gene (ampicillin resistance) and a NotI restriction site flanked by Frt sites was cloned into a cloning vector (pEGFP-N1, ClonTech, Palo Alto, CA) containing a marker for kanamycin resistance. The 200 bp genomic regions 5′ and 3′ to the coding ATG of the mouse Scn10a gene were cloned to flank the TRPV1 constructs. The fragments consisting of the HA-tagged mTRPV1 cassette and the flanking homology arms were released by restriction digestion. The purified fragment was inserted into a 230-kb-large bacterial artificial chromosome (BAC) containing the mouse *Scn10a* locus flanked by Not I sites in the pBeloBAC vector by ET recombination as described previously (Agarwal et al., 2004). The correctly recombined BACs were injected into pronuclei derived from C57BL6/j mouse strain (EMBL, Italy). Mice progeny thus obtained were further analyzed by genomic PCR and backcrossed into C57BL6/j mice genetic background. Mice were crossed with global TRPV1 knockout mice (TRPV1$^{-/-}$; Caterina and Julius, 2001; RRID:MGI:4418342) to generate mice specifically expressing HA-tagged wild-type mTRPV1 (SNS-mTRPV1^{wt}) or HA-tagged deSUMOylated mTRPV1 (SNS-mTRPV1^{K325A}) in sensory neurons.

Mouse tissue preparation

The animals were transcardially perfused with PBS followed by 4% PFA. The vertebral column and hind paw were extracted and post-fixed with 4%PFA for 24 hr. L3-L4 DRGs and paw skin were extracted and stored in 0.5% PFA. Prior to cryo-sectioning, the tissues were incubated overnight in 30% Sucrose solution at 4°C.

For immunoprecipitation studies, animals were sacrificed using CO_2 and tissue were immediately extracted and snap-frozen using liquid Nitrogen. The tissues were further stored at −80°C prior to analysis.

Mouse model of type 1 diabetes

Diabetes was induced by low dose multiple injections of STZ (60 mg/kg/d) in citrate buffer, intraperitoneally (i.p), in 8 wks-old C57BL6/j mice for 5 consecutive days. The control group was injected with citrate buffer alone. Blood glucose levels were measured once weekly in afternoon using a glucometer (Accu-Chek, Roche Diagnostics) for the entire course of the experiment. Mice with blood glucose levels above > 350 mg/dl were considered to be diabetic. The blood glucose levels were maintained in a range between 350 and 500 mg/dl by subcutaneous injection of insulin over the entire course of an experiment to ensure uniformity and consistency.

Behavioral measurements

All behavioral experiments were done in awake, unrestrained, acclimatized, age-matched adult mice. Mice were well habituated to the experimental setup twice a day for 3 days prior to the behavioral testing. We made all attempt to follow ARRIVE guidelines. The experimenter was blinded for the genotype or treatment of the groups tested in the experiments. Thermal sensitivity was measured using Hargreaves setup. The paw withdrawal latency was recorded on the application of infrared (IR) heat source on the plantar surface of mouse hind paw. A cut off of 20 s was set to avoid tissue burning. Two consecutive heat applications are performed at a time interval of 5 minutes. Von Frey measurements were done to assess mechanical sensitivity. Mice were placed on an elevated grid and von Frey monofilaments exerting a specific force of 0.07, 0.16, 0.4, 0.6, 1.0, 1.4, 2.0 and 4.0 g were applied for 5 times at time interval of 5 min on the plantar hindpaw. 40% response frequency was calculated as ''thresholds'' as described by Simonetti et al. (2014).

Plasmids and purified protein

The constructs expressing N-terminally hemagglutinin (HA)-tagged rTRPV1 as well as rTRPV1 mutants were cloned in the pIRES-AcGFP vector (ClonTech, Palo Alto, CA). The plasmids encoding Myc-DKK-tagged GAPDH and SENP1 were bought from OriGene Technologies (Inc. Rockville, MD). The His6SUMO-SENP1 catalytic domain was purchased from Boston Biochem.

Please cite this article in press as: Agarwal et al., SUMOylation of Enzymes and Ion Channels in Sensory Neurons Protects against Metabolic Dysfunction, Neuropathy, and Sensory Loss in Diabetes, Neuron (2020), https://doi.org/10.1016/j.neuron.2020.06.037

Antibodies

A list of antibodies used in this study can be found in Table S5.

Cell surface protein expression

HEK293 cells were transfected with HA-Tagged rat TRPV1 (rTRPV1) constructs. The surface proteins were biotinylated using Pierce® Cell surface protein isolation kit. Briefly, the transfected cells were washed with ice-cold PBS and labeled with 250 μg Sulfo-NHS-SS Biotin for 30 minutes at 4°C. The cells were washed with TBS and lysate were prepared as per kit manufacture protocols. The lysis buffer was supplemented with NEM.

The surface targeting of HA-tagged rTRPV1 constructs was analyzed by labeling the plasma membrane of transfected HEK cells with Wheat Germ Agglutinin (WGA) conjugated to Alexa Fluro®-647 (Invitrogen). The cells were washed with ice-cold PBS. The cells were incubated in 5 μg/ml WGA-fluor®647 (Life technologies) in HBSS and incubated for 10 minutes at 37°C. The cells were washed, fixed using 4% PFA solution and further stained with specific antibodies.

Immunoprecipitation and western blot analysis

Immunoprecipitation was done either from mouse/human tissues or from HEK293 cells using the protocol described by Becker et al. (2013). The cells or tissue material were lysed in 1% Sodium dodecyl sulfate (SDS) lysis buffer supplemented with N-ethylmaleimide (NEM). The lysate was diluted to 0.1% SDS concentration prior to immunoprecipitation. Lysates or Immunoprecipitated proteins were resolved on SDS-PAGE and transferred to nitrocellulose membrane. Membranes were incubated with specific primary and secondary antibodies as per standard protocol. The protein(s) specific bands were detected using Lumi-Light^{plus}, Roche, Germany. All results were verified from three independent experiments.

In vitro SUMOylation assay

In vitro SUMOylation assay was performed using SUMOlink^{TM} assay kit (Active motif). The manufacturer's protocol was followed for setting up the reaction. Briefly, the respective purified proteins of interest were incubated either with SUMO1 (wild-type) or with SUMO 1 (mutant) in SUMOylation buffer and incubated for 4 hr at 30°C. The reaction was terminated by addition of SDS-PAGE loading buffer and the products were analyzed via SDS-PAGE.

Site-directed mutagenesis

SUMOylation site in TRPV1 and GAPDH were analyzed by mutating lysine residue to Alanine/Arginine using GeneArt® Site-Directed Mutagenesis System, Life Technologies. All mutant plasmids were verified by sequencing.

Calcium imaging

HA-rTRPV1-IRES-AcGFP constructs were transfected into HEK293 cells cultured on poly L-lysine coated glass coverslips. After 48 hr. of transfections, transfected HEK293 cells were loaded with Fura-2 (1 μM) for 30 min. After 30 min of de-esterification, calcium signals were recorded on the application of capsaicin (1 μM) in perfusion buffer in continuous mode for the indicated time. Recordings of calcium signals was done using upright fluorescence Olympus BX51WI microscope (Olympus, Japan) with 16X objective using Sensicam CCD camera (PCO) on TILLvisION software. F340/380 ratios were calculated as described in Luo et al. (2012) only in GFP positive cells.

DRG cultures were prepared as described above. DRG neurons were loaded with 5 μM Fura-2-AM for 20 min in recording buffer (4 mM KCl, 140 mM NaCl, 1 mM MgCl2, 2 mM CaCl2, 4 mM Glucose, 10 mM HEPES). In experiments investigating the impact of lactate and methylglyoxal on capsaicin-evoked calcium transients, the DRG culture were incubated with lactate (3 mM) or methylglyoxal (100 μM) for 30 min prior to imaging. Loaded cells were then imaged with a ProgRes MF cool camera (Jenoptik) mounted on an Olympus BX51WI microscope. ValveLink 8.2 perfusion system (AutoMate Scientific) and image acquisition were controlled by a HEKA double patch clamp EPC10 amplifier driven with the PatchMaster image extension (HEKA). A Pharmacia LKB peristaltic pump removed the excess of the buffer. 340 and 380 nm wavelength light was generated by the Polychrome V monochromator (Till Photonics). Prior stimulation, CdCl2 (100 μM) was added to the buffer to block calcium entry through voltage-regulated calcium channels. Capsaicin (200 nM) and KCl (50 mM) were applied for 5 s with the perfusion tip close to the cells followed by washing with recording buffer. Ten seconds before stimulations and for 50 s, 340 and 380 nM images were acquired at 0.5 s interval. After that, one image was acquired every 5 s to avoid fluorescence bleaching. 340/380 ration values were obtained with ImageJ and the resulting data analyzed with Prism (GraphPad Software).

Immunohistochemistry

Immunohistochemistry was performed as described in Vicuña et al. (2015). Briefly, the tissue sections were fixed and permeabilized in 0.5% PBST, washed and blocked with Horse serum (HS). The sections were incubated overnight with appropriate primary antibody in 7% HS in 1x PBS at 4°C. Subsequently, on the next day, sections were washed and incubated in Alexa Fluor 488- or Alexa Fluor 594 conjugated secondary antibody. Further, the sections were washed and mounted in Mowiol. Fluorescence images were obtained using a laser-scanning spectral confocal microscope (Leica TCS SP8 AOBS, Bensheim, Germany). Sequential scans were performed when labeled scanned for more than 1 fluorophore.

Activity assays

Activity assays were performed either from diabetic or non-diabetic tissue samples or from culture HEK cells under different glucose concentration. HEK cells were culture either with 5.5 mM glucose concentration or with 25 mM glucose concentration. The cells were cultured for 8 wks to mimic the prolonged hyperglycemia effect *in vivo* and the activity assays were performed thereafter. To control for high osmolarity, another batch of cells was treated for equal period of time with mannitol (19.5 mM) and glucose (5.5 mM). In all activity assays, normalization to expression of control protein (tubulin) was undertaken prior to final quantification of activity.

GAPDH activity assay

The GAPDH activity was measured using ScienCell™ colorimetric GAPDH assay kit. GAPDH activity assay kit based on the oxidation of β-NADH to β-NAD in the presence of 3-phophoglyceric acid, ATP and GAPDH. The manufacturer's protocol was performed to measure the activity of GAPDH in transfected HEK cells of mouse tissue. The cells or tissue were lysed in cell lysis buffer from the kit. The protein concentration was measured using Bradford assay and the equal amount of total protein from different samples was serially diluted in duplicates and GAPDH activity was determined by assaying the rate of NADH oxidation by measuring the reduction in absorbance at 340 nm.

Citrate synthase activity assay

The citrate synthase activity was measurement using **c**itrate synthase activity assay kit from Sigma Aldrich. Manufacture protocol was followed for activity determination from cultured HEK cells. Briefly, HEK cells are washed with pre-warmed PBS, trypsinized, triturated and resuspended with the culturing media. The cell number is counted in a Neubauer chamber, centrifuged and resuspended in assay buffer. The equal number of cells was taken between different samples.

Aldehyde Dehydrogenase (ALDH) activity assay

The ALDH activity was determined using Aldehyde Dehydrogenase activity colorimetric assay kit from Sigma Aldrich. ALDH activity is determined by a coupled enzyme assay in which ALDH oxidized aldehyde and generate NADH which reacts with the probe to generate the colorimetric product which can be measured at an absorbance at 450 nm. The cells were lysed in the assay buffer provided with the kit. Samples were prepared as described before.

Transketolase activity assay

The activity of transketolase (TK) and transketolase like (TKTL) protein are measured by the enzyme kinetic method based on Chamberlain et al. (1996), using d-ribose-5-phosphate in excess as the sole substrate. Briefly, HEK-cells were lysed and mixed with either a normal substrate cocktail (30 mM R-5-P, 253 M μNADH, 185 U/ml TPI, 7.5 U/ml GDH) or a substrate cocktail with 350 μM TPP. Subsequently, the absorbance is monitored at 340 nm every 10 minutes for at least 2 hours. The linear decrease (slope) against the time represents the rate of NADH oxidation and further the relative activity of transketolase.

Mass-spectrometry analysis (LC/MS-MS)

DRG tissue was extracted from C57BL6 mice. All DRGs from single mouse was pooled to one sample. Total of 4 samples was analyzed per experimental condition. The tissue samples were lysed as described before. Immunoprecipitates obtained using either anti-SUMO 1 antibody or anti-GFP antibody were subjected to LC MS/MS as described in Njoo et al. (2015). Briefly, samples were subjected to LC MS/MS analysis using a nanoHPLC system (Eksigent, Axel Semrau) coupled with a ESI LTQ Orbitrap mass spectrometer (Thermo Fischer). MS data was evaluated using rPQ score as described in Berkefeld et al. (2006). rPQ score is the ratio of peptide queries obtained from any protein from the immunoprecipitates using anti-SUMO1 antibody and control GFP antibody.

Metabolite analysis by GC/MS

The mouse tissues were extracted and snap freeze as described above. Frozen material was extracted with 100% methanol for 15 min at 70°C. 5 μl Ribitol (0.2 mg/ml) was added as internal standard to each sample. Chloroform was added and samples were shaken at 37°C for 5 min. Subsequently, aqueous phase was separated and lyophilized. Pellets were re-dissolved in 20 μl methoximation reagent containing 20 mg/ml methoxyamine hydrochloride (Sigma 226904) in pyridine (Sigma 270970) and incubated for 2 h at 37°C with shaking. For silylation, 32.2 μl N-Methyl-N-(trimethylsilyl)trifluoroacetamide (MSTFA; Sigma M7891) and 2.8 μl Alkane Standard Mixture (50 mg/ml C_{10} - C_{40}; Fluka 68281) were added to each sample. After incubation for 30 min at 50°C, samples were transferred to glass vials for GC/MS analysis. GC/MS-QP2010 Plus (Shimadzu®) fitted with a Zebron ZB 5MS column (Phenomenex®; 30 m x 0.25 mm x 0.25 μm) was used for GC/MS analysis. The "GCMS solution" software (Shimadzu®) was used for data processing.

In silico prediction of SUMOylation sites

SUMOSP 2.0 (Zhao et al., 2014) and SUMOplot™ (developed by Abgent) analysis program were used to predict the potential SUMOylation site in the target protein sequence. The SUMOplot analysis program predicts the probability for the SUMO consensus sequence (SUMO-CS) to be engaged in SUMO attachment. SUMOSP program predicts both covalent SUMOylation sites and non-covalent SUMOylation motif.

Human tissue

Human sciatic materials were provided by the tissue bank of the National Centre for Tumor Diseases (NCT, Heidelberg, Germany). All patient specimen and corresponding clinical data were provided in a pseudonymized form according to the standard operating procedures of the tissue bank and upon the approval by the ethics committee of Heidelberg University (Ethic votes 206/2005 and 207/2005). The samples were snap frozen immediately upon surgical removal and stored in the certified and bench-marked NCT biobank. At the time of experiments, frozen samples were pulverized under liquid nitrogen and then transferred to 1% SDS lysis buffer supplemented with NEM. The lysate was diluted to 0.1% SDS concentration prior to immunoprecipitation. The immunoprecipitation studies were done as described before.

QUANTIFICATION AND STATISTICAL ANALYSIS

Student's t test was employed while comparing two genetic groups with each other for a single parameter and single time point. Analysis of variance (ANOVA) for random measures or repeated-measures was employed, as appropriate, in experiments comparing multiple groups or multiple time points and post hoc Tukey's test for multiple comparisons was performed. The exact statistical test employed for each dataset is indicated in the figure legends. All data in the figures are expressed as mean ± SEM.

ADDITIONAL RESOURCES

This study has not contributed any resource to a new website or forum.

Neuron, Volume *107*

Supplemental Information

SUMOylation of Enzymes and Ion Channels in Sensory Neurons Protects against Metabolic Dysfunction, Neuropathy, and Sensory Loss in Diabetes

Nitin Agarwal, Francisco J. Taberner, Daniel Rangel Rojas, Mirko Moroni, Damir Omberbasic, Christian Njoo, Alexandra Andrieux, Pooja Gupta, Kiran K. Bali, Esther Herpel, Faramarz Faghihi, Thomas Fleming, Anne Dejean, Stefan G. Lechner, Peter P. Nawroth, Gary R. Lewin, and Rohini Kuner

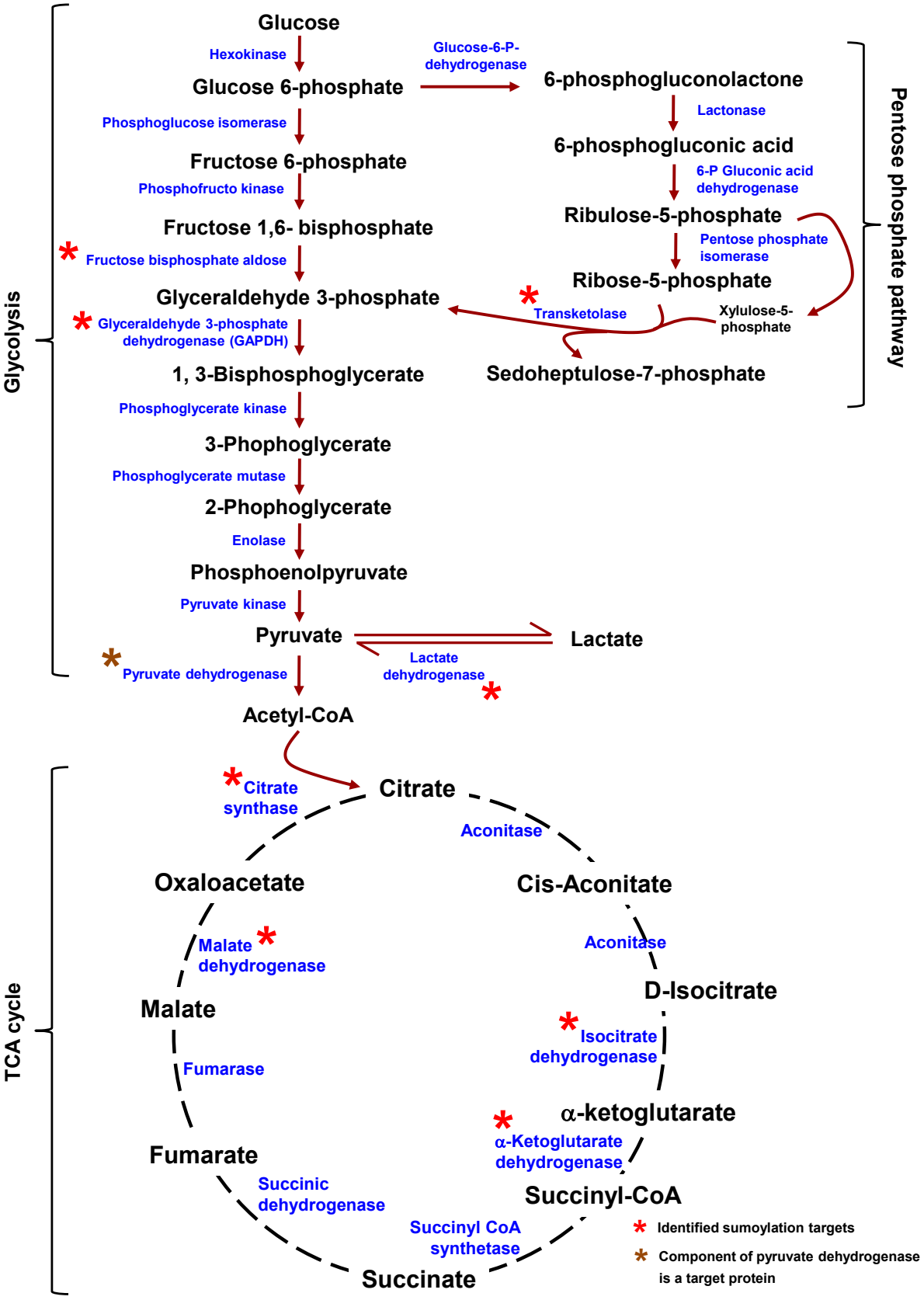

Supplementary figure 1 (related to figure 1): Detailed overview of the known steps, enzymes and metabolites of the glycolysis pathway, the Kreb's cycle (TCA) and pentose phosphate pathway and depiction of enzymes that were identified to be putative targets of SUMOylation in mouse DRG (indicated by asterisks).

A

Potential sumoylation sites predicted in GAPDH protein sequence

Lysine position	Site	*SumoSP*	
59	GTV**K**AEN	2.882	Type I: Ψ-K-X-E
257	DDI**K**KVV	2.676	Type II: Non-consensus
332	MAS**K**E	3.118	Type II: Non-consensus

B

Conditional deletion of sumoylation in peripheral sensory neurons

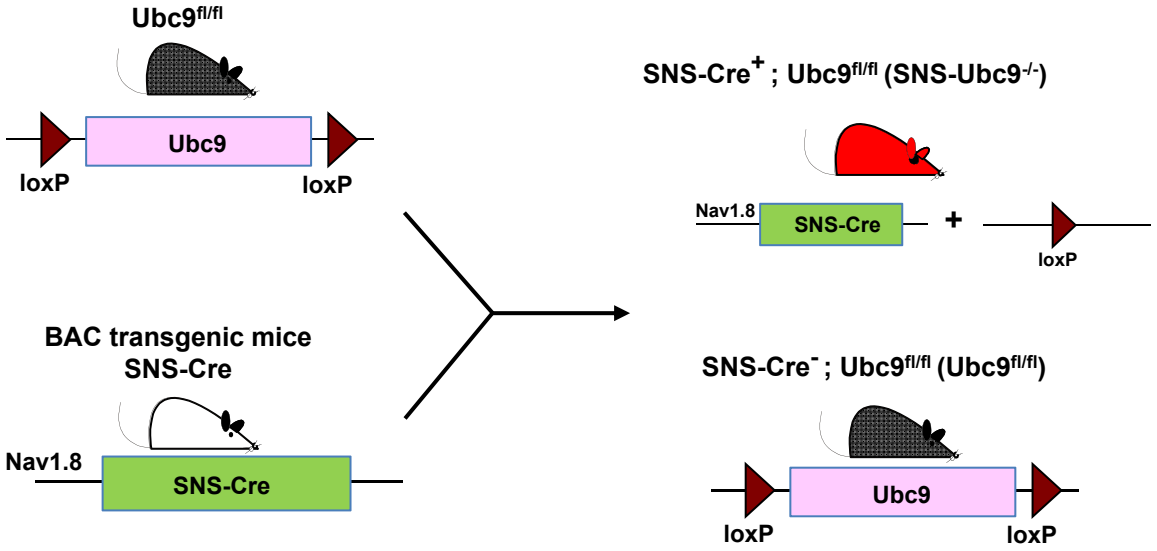

C

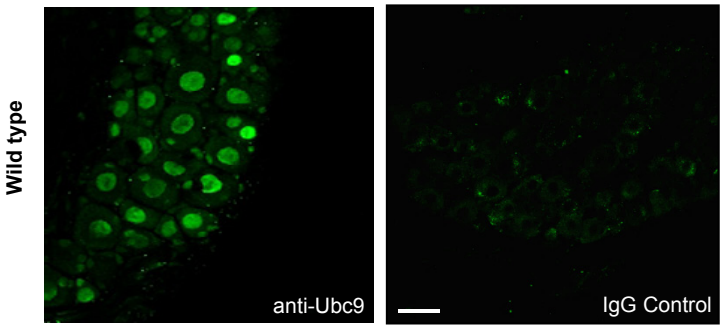

Supplementary figure 2 (related to figure 1 and 3): *In silico* analysis of putative SUMOylation sites in GAPDH and generation and characterization of mice lacking SUMOylation in DRG neurons. (A) Overview on the consensus sites for SUMOylation detected in GAPDH protein Likely SUMOylated lysines are indicated in red. (B) Strategy for generation of conditionally targeted mice lacking Ubc9 selectively in DRG neurons using SNS-Cre mice expressing the Cre recombinase under the influence of the Nav1.8 promoter and mice carrying floxed allelel of the *Ubc9* gene. (C) Negative controls for anti-Ubc9 immunostaining with secondary antibody alone.

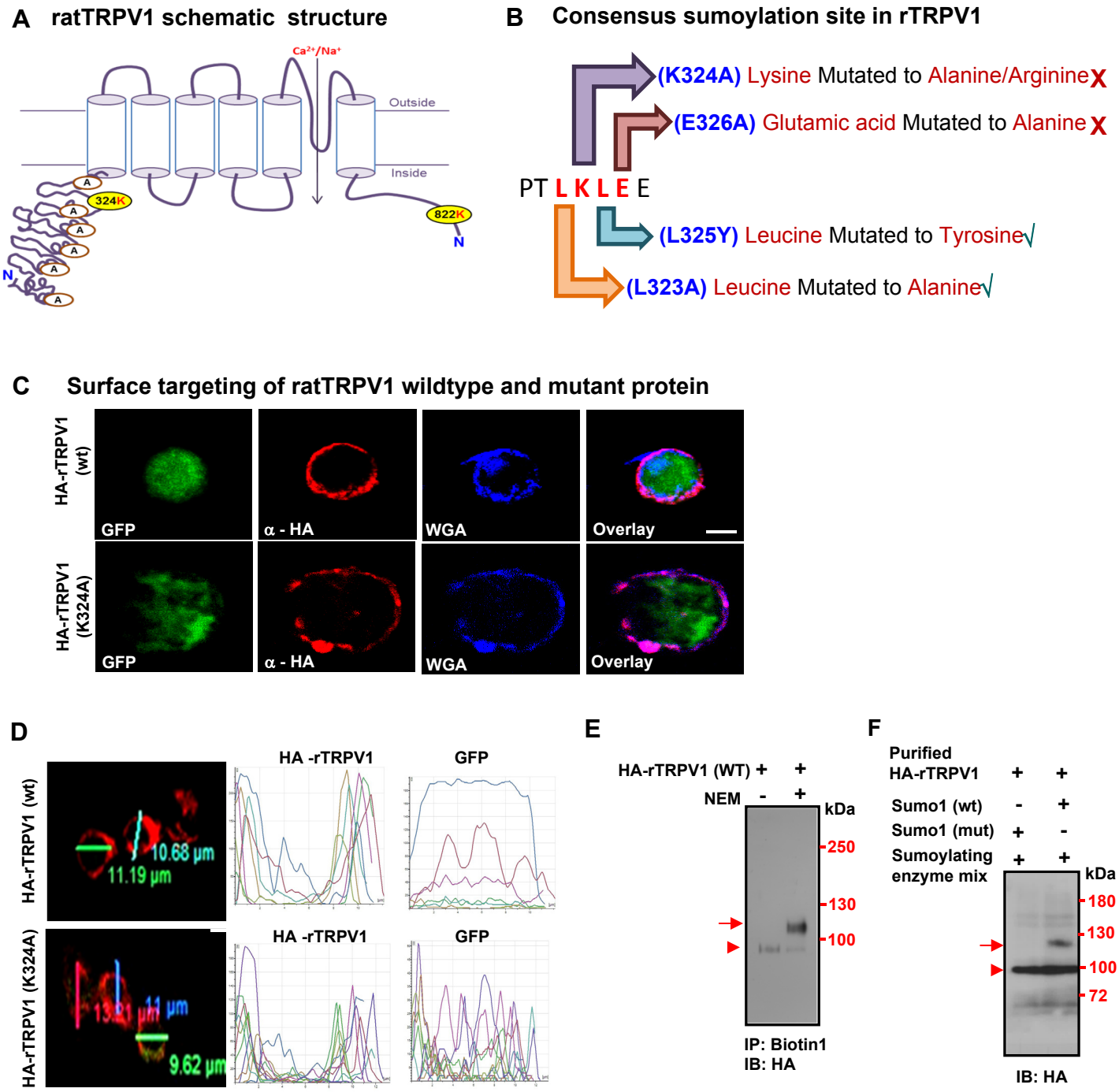

Supplementary figure 3 (related to figure 5): Additional information and controls for validation of SUMOylation of rTRPV1. (A) Overview of the positioning two potential SUMOylation sites in the structure of rTRPV1. The site which was validated by results described here to be the bonafide site (K324) is located in the proximity of the ankyrin repeats (denoted by A) in the intracellular N-terminus of rTRPV1. (B) Strategy for mutational analysis of the consensus site for rTRPV1 involving K324. Shown are the amino acids that were mutated and the predicted outcomes (X: SUMOylation unchanged; √ SUMOylation disrupted) that would confirm K324 as the bonafide SUMOylation site. (C) Analysis of surface localisation of rTRPV1 expressed in HEK cells either in the wildtype form (Wt) or K324A mutant form, both HA-tagged and co-expressing GFP. Anti-HA immunohistochemistry was combined with immunostaining for Wheat Germ Agglutinin (WGA), which is a cell surface marker. Scale bar = 5 µM. (D) The localisation of wt rTRPV1 and K324A rTRPV1 at the cell surface was further confirmed via studying line profiles in confocal images (left), which showed typical line profiles (traces on the right) characterised by high signals at the two ends of the cellular width (corresponding to membrane localisation) with TRPV1 whereas the line profile of intracellularly localised GFP showed signals in the middle (corresponding to cytoplasmic localisation). Scale bar = 10 µM. (E) A representative blot showing change in proportion of SUMOylated TRPV1 in presence or absence of NEM. (F) *In vitro* sumoylation assay performed on purified HA-tagged rTRPV1. Arrow and arrowhead indicate the SUMOylated and unSUMOylated forms of TRPV1, respectively

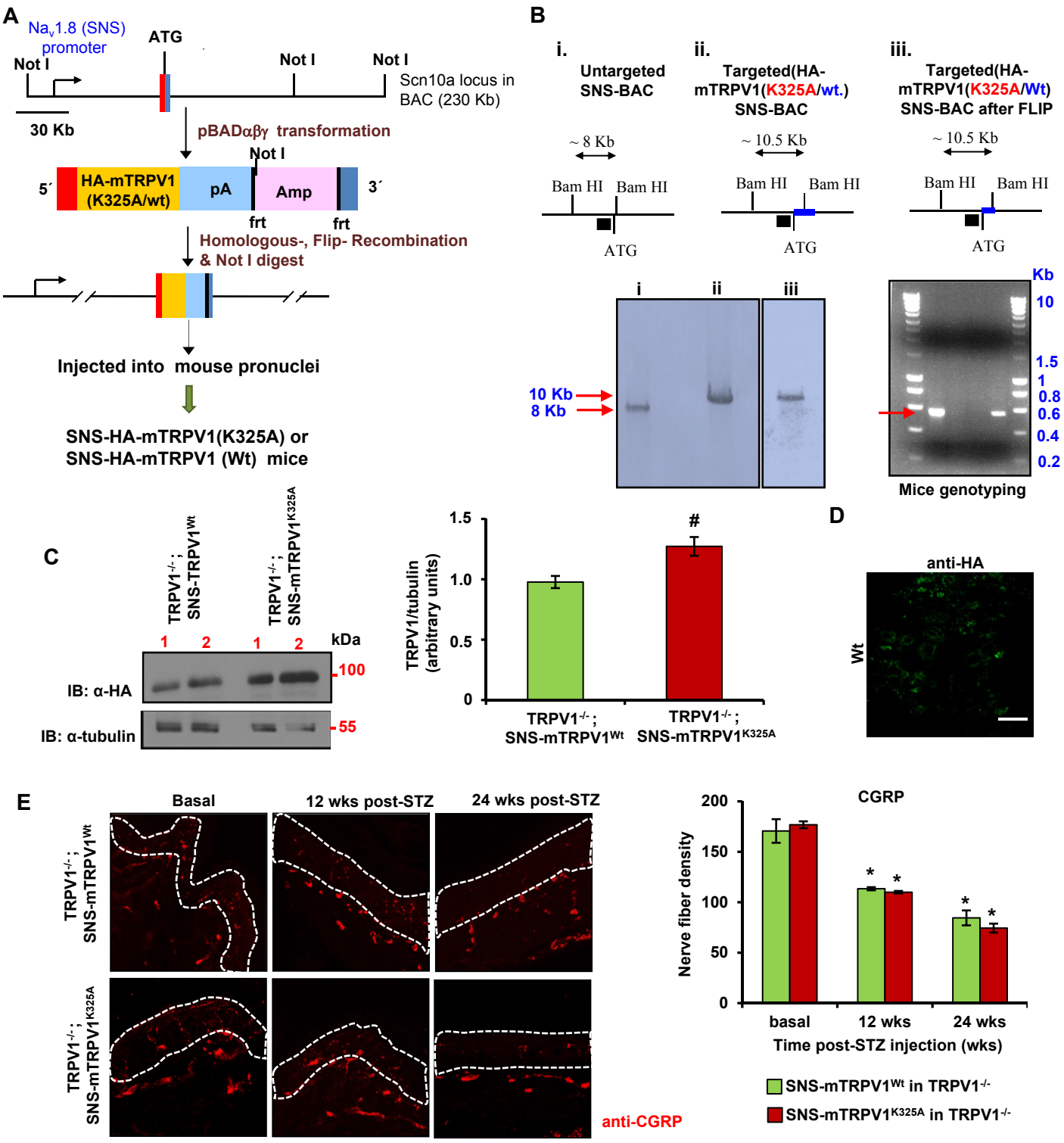

Supplementary figure 4 (related to figure 7): Generation and characterisation of mice transgenically expressing SUMOylation-deficient or wildtype versions of mouse TRPV1 (mTRPV1)(TRPV1$^{-/-}$; SNS-mTRPV1^{K325A} mice and TRPV1$^{-/-}$; SNS-mTRPV1^{Wt} mice, respectively). (A) Targeting of wildtype or K325A mutant forms of mTRPV1 into start codon of mouse *Scn10a* gene (encoding Nav1.8) in a bacterial artificial chromosome; (B) Strategy and results for Southern blotting analyses for confirmation of correct targeting; (C) Quantitative estimation of the expression of HA-tagged mTRPV1 in sciatic nerve of mice transgenically expressing SUMOylation-deficient mTRPV1 or wildtype mTRPV1 (crossed into the mTRPV1$^{-/-}$ background). Shown are a typical example of Western blotting and quantitative summary from 3 independent experiments. (D) Negative control for anti-HA staining on DRG sections of wildtype mice. (E) Typical examples and quantitative summary of immunolabeling for the peptidergic nociceptive nerve marker, CGRP, in nerve endings in the epidermis (areas demarcated by dashed lines) of the plantar paw skin of TRPV1$^{-/-}$; SNS-mTRPV1^{K325A} mice and TRPV1$^{-/-}$; SNS-mTRPV1^{Wt} (control) mice prior to and over 24 wks after induction of diabetes. In E, # indicates $p<0.05$ compared across genotypes for the same treatment; * indicates $p<0.05$ as compared to basal; ANOVA of repeated measures, followed by post-hoc Tukey's test was employed. Scale bars represent 25 μm in panel E. Data represent mean ± S.E.M.

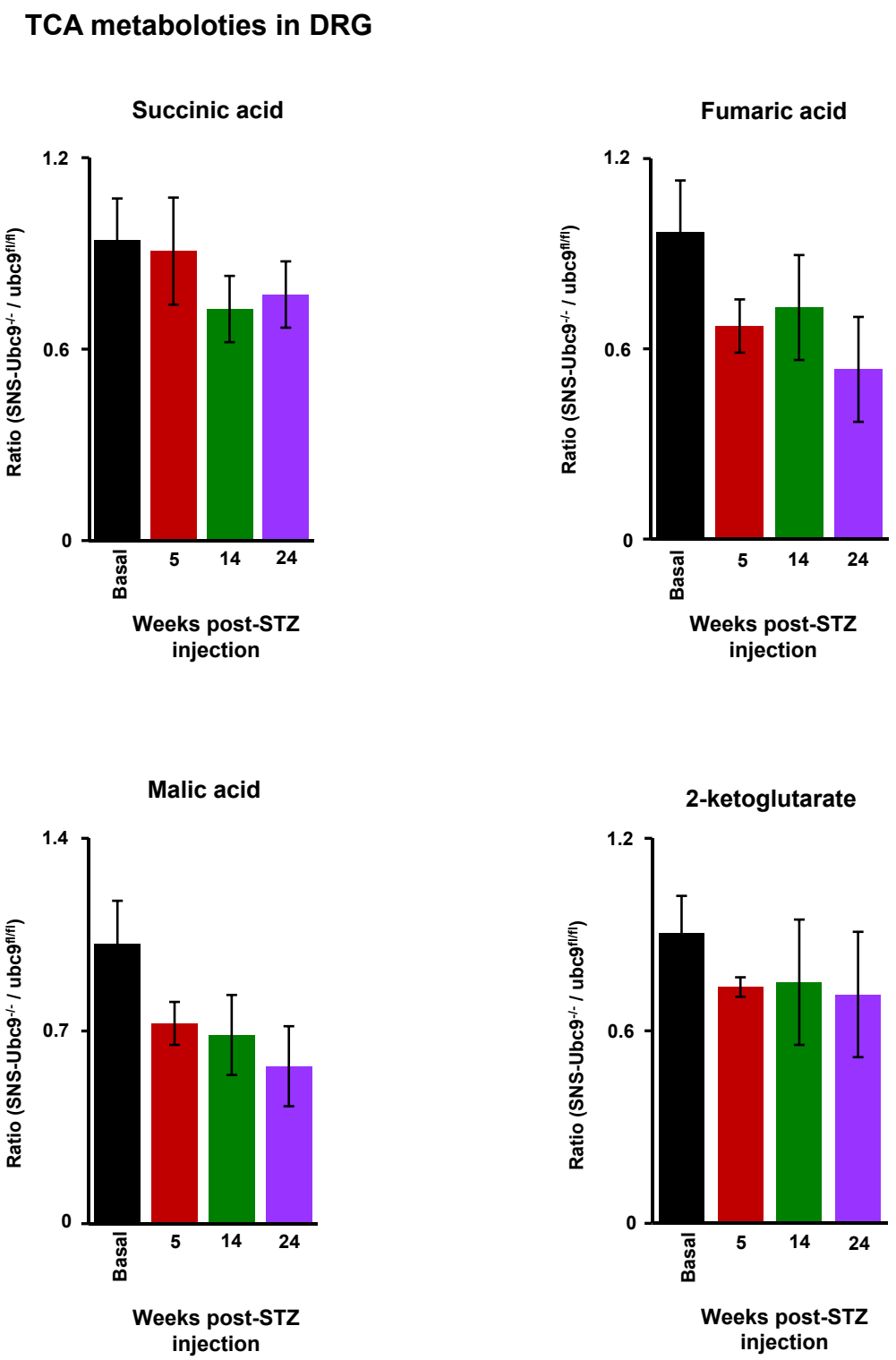

Supplementary figure 5 (related to figure 4): LC-MS-based estimation of TCA metabolites in DRGs before or after at 5, 14 and 24 wks post-STZ treatment in SNSUbc9$^{-/-}$ mice and Ubc9$^{fl/fl}$ mice. Data are shown as ratios of levels between SNS-Ubc9$^{-/-}$ and control Ubc9$^{fl/fl}$ mice under non-diabetic and diabetic conditions. Data represent mean ± S.E.M.

Supplementary table 1 related to figure 1

SN	Identified Proteins	Accession Number	Molecular Weight	rPQ	
1	1-phosphatidylinositol 4,5-bisphosphate phosphodiesterase zeta-1 OS=Mus musculus GN=Plcz1 PE=1 SV=1	PLCZ1_MOUSE	75 kDa	55.5	Neuronal and non-neuronal
2	2-oxoglutarate dehydrogenase, mitochondrial OS=Mus musculus GN=Ogdh PE=1 SV=3	ODO1_MOUSE	115 kDa	20.25	Neuronal and non-neuronal
3	3-ketoacyl-CoA thiolase, mitochondrial OS=Mus musculus GN=Acaa2 PE=1 SV=3	THIM_MOUSE	41 kDa	29.25	Neuronal and non-neuronal
4	78 kDa glucose-regulated protein OS=Mus musculus GN=Hspa5 PE=1 SV=3	GRP78_MOUSE	72 kDa	29	Neuronal and non-neuronal
5	A disintegrin and metalloproteinase with thrombospondin motifs 8 OS=Mus musculus GN=Adamts8 PE=2 SV=1	ATS8_MOUSE	99 kDa	10.25	Non-neuronal
6	Acetyl-CoA acetyltransferase, mitochondrial OS=Mus musculus GN=Acat1 PE=1 SV=1	THIL_MOUSE	45 kDa	17.75	Neuronal and non-neuronal
7	Actin, cytoplasmic 1 OS=Mus musculus GN=Actb PE=1 SV=1	ACTB_MOUSE	42 kDa	43.75	Neuronal and non-neuronal
8	Acyl-coenzyme A thioesterase THEM5 OS=Mus musculus GN=Them5 PE=2 SV=1	ACO15_MOUSE	28 kDa	13.25	Neuronal and non-neuronal
9	Adenosine deaminase-like protein OS=Mus musculus GN=Adal PE=2 SV=1	ADAL_MOUSE	41 kDa	17	Neuronal and non-neuronal
10	Adenylate cyclase type 10 OS=Mus musculus GN=Adcy10 PE=2 SV=2	ADCYA_MOUSE	186 kDa	11.5	Neuronal and non-neuronal
11	ADP/ATP translocase 4 OS=Mus musculus GN=Slc25a31 PE=2 SV=1	ADT4_MOUSE	41 kDa	23.25	Neuronal and non-neuronal
12	Aldehyde dehydrogenase, dimeric NADP-preferring OS=Mus musculus GN=Aldh3a1 PE=2 SV=2	AL3A1_MOUSE	50 kDa	38	Neuronal and non-neuronal
13	Alpha-2-macroglobulin-P OS=Mus musculus GN=A2mp PE=2 SV=2	A2MP_MOUSE	164 kDa	8.5	Neuronal and non-neuronal
14	Alpha-N-acetylneuraminide alpha-2,8-sialyltransferase OS=Mus musculus GN=St8sia1 PE=1 SV=2	SIA8A_MOUSE	40 kDa	5	Neuronal and non-neuronal
15	Annexin A2 OS=Mus musculus GN=Anxa2 PE=1 SV=2	ANXA2_MOUSE	39 kDa	14.75	Neuronal and non-neuronal
16	Arf-GAP with SH3 domain, ANK repeat and PH domain-containing protein 2 OS=Mus musculus GN=Asap2 PE=1 SV=3	ASAP2_MOUSE	107 kDa	20.5	Neuronal and non-neuronal
17	Aspartate aminotransferase, mitochondrial OS=Mus musculus GN=Got2 PE=1 SV=1	AATM_MOUSE	47 kDa	15	Neuronal and non-neuronal
18	ATP-dependent DNA helicase Q4 OS=Mus musculus GN=Recql4 PE=2 SV=2	RECQ4_MOUSE	135 kDa	24	Neuronal and non-neuronal
19	B box and SPRY domain-containing protein OS=Mus musculus GN=Bspry PE=1 SV=1	BSPRY_MOUSE	53 kDa	15	Non-neuronal
20	Basement membrane-specific heparan sulfate proteoglycan core protein OS=Mus musculus GN=Hspg2 PE=1 SV=1	PGBM_MOUSE	398 kDa	14.75	Non-neuronal
21	Cadherin EGF LAG seven-pass G-type receptor 3 OS=Mus musculus GN=Celsr3 PE=2 SV=2	CELR3_MOUSE	358 kDa	14.25	Neuronal
22	Ceruloplasmin OS=Mus musculus GN=Cp PE=1 SV=2	CERU_MOUSE	121 kDa	11	Neuronal and non-neuronal
23	Chromatin modification-related protein MEAF6 OS=Mus musculus GN=Meaf6 PE=2 SV=1	EAF6_MOUSE	22 kDa	13	Neuronal and non-neuronal
24	Circadian locomoter output cycles protein kaput OS=Mus musculus GN=Clock PE=1 SV=1	CLOCK_MOUSE	96 kDa	13.25	Neuronal and non-neuronal
25	Citrate synthase, mitochondrial OS=Mus musculus GN=Cs PE=1 SV=1	CISY_MOUSE	52 kDa	49.5	Neuronal and non-neuronal
26	Claudin-22 OS=Mus musculus GN=Cldn22 PE=2 SV=1	CLD22_MOUSE	24 kDa	8.5	Neuronal and non-neuronal
27	Coiled-coil domain-containing protein 97 OS=Mus musculus GN=Ccdc97 PE=1 SV=1	CCD97_MOUSE	39 kDa	13.5	Neuronal and non-neuronal
28	Collagen alpha-1(I) chain OS=Mus musculus GN=Col1a1 PE=1 SV=4	CO1A1_MOUSE	138 kDa	17.25	Neuronal and non-neuronal
29	Collagen alpha-1(II) chain OS=Mus musculus GN=Col2a1 PE=1 SV=2	CO2A1_MOUSE	142 kDa	16.75	Neuronal and non-neuronal
30	Collagen alpha-1(VI) chain OS=Mus musculus GN=Col6a1 PE=2 SV=1	CO6A1_MOUSE	108 kDa	23.5	Neuronal and non-neuronal
31	Collagen alpha-1(XXVIII) chain OS=Mus musculus GN=Col28a1 PE=2 SV=1	COSA1_MOUSE	119 kDa	19.5	Neuronal and non-neuronal
32	Collagen alpha-2(I) chain OS=Mus musculus GN=Col1a2 PE=2 SV=2	CO1A2_MOUSE	130 kDa	4.25	Neuronal and non-neuronal
33	Collagen alpha-2(IV) chain OS=Mus musculus GN=Col4a2 PE=2 SV=4	CO4A2_MOUSE	167 kDa	28.75	Neuronal and non-neuronal
34	Collagen alpha-2(VI) chain OS=Mus musculus GN=Col6a2 PE=2 SV=3	CO6A2_MOUSE	110 kDa	17.25	Neuronal and non-neuronal
35	Complement factor B OS=Mus musculus GN=Cfb PE=1 SV=2	CFAB_MOUSE	85 kDa	16.75	Neuronal and non-neuronal
36	Cysteine and histidine-rich protein 1 OS=Mus musculus GN=Cyhr1 PE=1 SV=1	CYHR1_MOUSE	36 kDa	17.55	Neuronal and non-neuronal
37	Cytochrome b-c1 complex subunit 2, mitochondrial OS=Mus musculus GN=Uqcrc2 PE=1 SV=1	QCR2_MOUSE	48 kDa	18.3	Neuronal and non-neuronal
38	Cytoplasmic aconitate hydratase OS=Mus musculus GN=Aco1 PE=1 SV=3	ACOC_MOUSE	98 kDa	11.85	Neuronal and non-neuronal
39	Cytosolic carboxypeptidase 4 OS=Mus musculus GN=Agbl1 PE=1 SV=2	ACOC_MOUSE	109 kDa	10.55	Neuronal and non-neuronal
40	Death-associated protein kinase 1 OS=Mus musculus GN=Dapk1 PE=1 SV=3	DAPK1_MOUSE	161 kDa	9.95	Neuronal and non-neuronal
41	Dehydrogenase/reductase SDR family member 1 OS=Mus musculus GN=Dhrs1 PE=2 SV=1	DHRS1_MOUSE	34 kDa	14.25	Neuronal and non-neuronal
42	Delta-1-pyrroline-5-carboxylate synthase OS=Mus musculus GN=Aldh18a1 PE=2 SV=2	P5CS_MOUSE	87 kDa	10.5	Neuronal and non-neuronal
43	Desmoglein-1-beta OS=Mus musculus GN=Dsg1b PE=1 SV=1	DSG1B_MOUSE	114 kDa	7.45	Neuronal and non-neuronal
44	Desmoplakin OS=Mus musculus GN=Dsp PE=2 SV=1	DESP_MOUSE	333 kDa	12	Neuronal and non-neuronal
45	Diacylglycerol kinase zeta OS=Mus musculus GN=Dgkz PE=1 SV=2	DGKZ_MOUSE	104 kDa	19.5	Neuronal and non-neuronal
46	Dihydrolipoyllysine-residue acetyltransferase component of pyruvate dehydrogenase complex, mitochondrial OS=Mus musculus GN=Dlat PE=1 SV=2	ODP2_MOUSE	68 kDa	9.75	Neuronal and non-neuronal
47	DNA helicase MCM9 OS=Mus musculus GN=Mcm9 PE=1 SV=2	MCM9_MOUSE	126 kDa	21	Neuronal and non-neuronal
48	DNA topoisomerase 2-binding protein 1 OS=Mus musculus GN=Topbp1 PE=1 SV=2	TOPB1_MOUSE	169 kDa	18.5	Neuronal and non-neuronal
49	DNA-dependent protein kinase catalytic subunit OS=Mus musculus GN=Prkdc PE=1 SV=3	PRKDC_MOUSE	471 kDa	10.06	Neuronal and non-neuronal
50	Dual specificity protein kinase CLK3 OS=Mus musculus GN=Clk3 PE=1 SV=2	CLK3_MOUSE	74 kDa	6	Neuronal and non-neuronal
51	Elongation factor 1-gamma OS=Mus musculus GN=Eef1g PE=1 SV=3	EF1G_MOUSE	50 kDa	32.175	Neuronal and non-neuronal
52	Elongation factor 2 OS=Mus musculus GN=Eef2 PE=1 SV=2	EF2_MOUSE	95 kDa	14.225	Neuronal and non-neuronal
53	Ephrin type-A receptor 8 OS=Mus musculus GN=Epha8 PE=1 SV=2	EPHA8_MOUSE	111 kDa	9	Neuronal
54	Exonuclease 1 OS=Mus musculus GN=Exo1 PE=2 SV=2	EXO1_MOUSE	92 kDa	2.5	Neuronal and non-neuronal
55	Filamin A-interacting protein 1-like OS=Mus musculus GN=Filip1l PE=1 SV=2	FIL1L_MOUSE	130 kDa	2.6	Neuronal and non-neuronal
56	Fructose-bisphosphate aldolase A OS=Mus musculus GN=Aldoa PE=1 SV=2	ALDOA_MOUSE	39 kDa	28.9	Neuronal and non-neuronal
57	Glutaredoxin-3 OS=Mus musculus GN=Glrx3 PE=1 SV=1	GLRX3_MOUSE	38 kDa	6.45	Neuronal and non-neuronal
58	Glyceraldehyde-3-phosphate dehydrogenase OS=Mus musculus GN=Gapdh PE=1 SV=2	G3P_MOUSE	36 kDa	42.5	Neuronal and non-neuronal
59	Glycogen phosphorylase, brain form OS=Mus musculus GN=Pygb PE=1 SV=3	PYGB_MOUSE	97 kDa	7.25	Neuronal and non-neuronal
60	Grancalcin OS=Mus musculus GN=Gca PE=2 SV=1	GRAN_MOUSE	25 kDa	9.46	Neuronal and non-neuronal
61	Heat shock 70 kDa protein 12A OS=Mus musculus GN=Hspa12a PE=1 SV=1	HS12A_MOUSE	74 kDa	30	Neuronal and non-neuronal
62	Heat shock cognate 71 kDa protein OS=Mus musculus GN=Hspa8 PE=1 SV=1	HSP7C_MOUSE	71 kDa	16.12	Neuronal and non-neuronal
63	Heat shock protein HSP 90-alpha OS=Mus musculus GN=Hsp90aa1 PE=1 SV=4	HS90A_MOUSE	85 kDa	24.5	Neuronal and non-neuronal
64	Heparan-sulfate 6-O-sulfotransferase 2 OS=Mus musculus GN=Hs6st2 PE=2 SV=3	H6ST2_MOUSE	69 kDa	7.51	Neuronal and non-neuronal
65	Heterogeneous nuclear ribonucleoproteins C1/C2 OS=Mus musculus GN=Hnrnpc PE=1 SV=1	HNRPC_MOUSE	34 kDa	4.76	Neuronal and non-neuronal
66	Hormone-sensitive lipase OS=Mus musculus GN=Lipe PE=1 SV=2	LIPS_MOUSE	83 kDa	3.87	Neuronal and non-neuronal
67	Hydrocephalus-inducing protein OS=Mus musculus GN=Hydin PE=2 SV=2	HYDIN_MOUSE	582 kDa	5.68	Neuronal and non-neuronal
68	Integrator complex subunit 11 OS=Mus musculus GN=Cpsf3l PE=2 SV=1	INT11_MOUSE	68 kDa	6	Neuronal and non-neuronal
69	Integrin alpha-E OS=Mus musculus GN=Itgae PE=2 SV=2	ITAE_MOUSE	129 kDa	9.75	Neuronal and non-neuronal
70	Integrin alpha-V OS=Mus musculus GN=Itgav PE=1 SV=2	ITAV_MOUSE	115 kDa	10.25	Neuronal and non-neuronal
71	Inter-alpha-trypsin inhibitor heavy chain H2 OS=Mus musculus GN=Itih2 PE=1 SV=1	ITIH2_MOUSE	106 kDa	3.5	Neuronal and non-neuronal
72	Interferon regulatory factor 5 OS=Mus musculus GN=Irf5 PE=1 SV=1	IRF5_MOUSE	56 kDa	4.5	Neuronal and non-neuronal
73	Isobutyryl-CoA dehydrogenase, mitochondrial OS=Mus musculus GN=Acad8 PE=2 SV=2	ACAD8_MOUSE	45 kDa	9.6	Neuronal and non-neuronal
74	Junction plakoglobin OS=Mus musculus GN=Jup PE=1 SV=3	PLAK_MOUSE	82 kDa	1.4	Neuronal and non-neuronal
75	Kinesin-like protein KIF13A OS=Mus musculus GN=Kif13a PE=1 SV=1	KI13A_MOUSE	196 kDa	5.68	Neuronal and non-neuronal
76	Kinesin-like protein KIF15 OS=Mus musculus GN=Kif15 PE=1 SV=1	KIF15_MOUSE	160 kDa	2.08	Neuronal and non-neuronal
77	Laminin subunit alpha-5 OS=Mus musculus GN=Lama5 PE=1 SV=4	LAMA5_MOUSE	404 kDa	8.13	Neuronal and non-neuronal
78	Laminin subunit beta-2 OS=Mus musculus GN=Lamb2 PE=2 SV=2	LAMB2_MOUSE	197 kDa	6.22	Neuronal and non-neuronal
79	L-lactate dehydrogenase B chain OS=Mus musculus GN=Ldhb PE=1 SV=2	LDHB_MOUSE	36 kda	7.87	Neuronal and non-neuronal
80	L-lactate dehydrogenase C chain OS=Mus musculus GN=Ldhc PE=1 SV=2	LDHC_MOUSE	36 kDa	4.75	Neuronal and non-neuronal
81	Lymphoid-restricted membrane protein OS=Mus musculus GN=Lrmp PE=1 SV=1	LRMP_MOUSE	60 kDa	0.37	Neuronal and non-neuronal
82	Lysozyme C-1 OS=Mus musculus GN=Lyz1 PE=1 SV=1	LYZ1_MOUSE	17 kDa	2.20	Neuronal and non-neuronal
83	Malate dehydrogenase, mitochondrial OS=Mus musculus GN=Mdh2 PE=1 SV=3	MDHM_MOUSE	35 kDa	8.25	Neuronal and non-neuronal
84	MAP7 domain-containing protein 3 OS=Mus musculus GN=Map7d3 PE=2 SV=1	MA7D3_MOUSE	98 kDa	5.25	Neuronal and non-neuronal
85	Microtubule-associated tumor suppressor 1 homolog OS=Mus musculus GN=Mtus1 PE=1 SV=2	MTUS1_MOUSE	134 kDa	4	Neuronal and non-neuronal
86	Myocardial zonula adherens protein OS=Mus musculus GN=Myzap PE=1 SV=1	MYZAP_MOUSE	54 kDa	4.16	Neuronal and non-neuronal
87	Myosin-10 OS=Mus musculus GN=Myh10 PE=1 SV=2	MYH10_MOUSE	229 kDa	3.15	Neuronal and non-neuronal
88	Myosin-8 OS=Mus musculus GN=Myh8 PE=1 SV=2	MYH8_MOUSE	223 kDa	8.33	Neuronal and non-neuronal
89	N6-adenosine-methyltransferase 70 kDa subunit OS=Mus musculus GN=Mettl3 PE=2 SV=2	MTA70_MOUSE	65 kDa	0.53	Non-neuronal
90	NAD(P) transhydrogenase, mitochondrial OS=Mus musculus GN=Nnt PE=1 SV=2	NNTM_MOUSE	114 kDa	5.76	Neuronal and non-neuronal
91	NADH-ubiquinone oxidoreductase 75 kDa subunit, mitochondrial OS=Mus musculus GN=Ndufs1 PE=1 SV=2	NDUS1_MOUSE	80 kDa	13.25	Neuronal and non-neuronal
92	Nebulin-related-anchoring protein OS=Mus musculus GN=Nrap PE=1 SV=3	NRAP_MOUSE	196 kDa	0.2	Neuronal and non-neuronal
93	Nestin OS=Mus musculus GN=Nes PE=1 SV=1	NEST_MOUSE	207 kDa	4.5	Neuronal and non-neuronal
94	Netrin-5 OS=Mus musculus GN=Ntn5 PE=2 SV=2	NET5_MOUSE	49 kDa	4.87	Neuronal and non-neuronal
95	Neurofilament heavy polypeptide OS=Mus musculus GN=Nefh PE=1 SV=3	NFH_MOUSE	117 kDa	13	Neuronal and non-neuronal
96	Neurofilament light polypeptide OS=Mus musculus GN=Nefl PE=1 SV=5	NFL_MOUSE	62 kDa	2.7	Neuronal
97	Neurofilament medium polypeptide OS=Mus musculus GN=Nefm PE=1 SV=4	NFM_MOUSE	96 kDa	2	Neuronal
98	Neurogenic locus notch homolog protein 4 OS=Mus musculus GN=Notch4 PE=1 SV=2	NOTC4_MOUSE	207 kDa	4.5	Neuronal and non-neuronal
99	Neuronal acetylcholine receptor subunit alpha-4 OS=Mus musculus GN=Chrna4 PE=2 SV=2	ACHA4_MOUSE	70 kDa	3.75	Neuronal and non-neuronal
100	Neuronal growth regulator 1 OS=Mus musculus GN=Negr1 PE=1 SV=1	NEGR1_MOUSE	38 kDa	1.32	Neuronal

101	Neurotrophin receptor-interacting factor 2 OS=Mus musculus GN=Nrif2 PE=1 SV=1	NRIF2_MOUSE	93 kDa	0.69375	Neuronal and non-neuronal
102	NFX1-type zinc finger-containing protein 1 OS=Mus musculus GN=Znfx1 PE=2 SV=3	ZNFX1_MOUSE	219 kDa	3.58	Neuronal and non-neuronal
103	Nidogen-1 OS=Mus musculus GN=Nid1 PE=1 SV=2	NID1_MOUSE	137 kDa	1.375	Neuronal and non-neuronal
104	Nidogen-2 OS=Mus musculus GN=Nid2 PE=1 SV=2	NID2_MOUSE	154 kDa	6	Neuronal and non-neuronal
105	Nipped-B-like protein OS=Mus musculus GN=Nipbl PE=1 SV=1	NIPBL_MOUSE	315 kDa	5.5	Neuronal and non-neuronal
106	Nitric oxide synthase, brain OS=Mus musculus GN=Nos1 PE=1 SV=1	NOS1_MOUSE	160 kDa	6	Neuronal and non-neuronal
107	Nuclear pore complex protein Nup214 OS=Mus musculus GN=Nup214 PE=1 SV=2	NU214_MOUSE	213 kDa	9.25	Neuronal and non-neuronal
108	Nuclear receptor coactivator 6 OS=Mus musculus GN=Ncoa6 PE=1 SV=1	NCOA6_MOUSE	220 kDa	4.25	Neuronal and non-neuronal
109	Nuclear receptor subfamily 4 group A member 2 OS=Mus musculus GN=Nr4a2 PE=1 SV=1	NR4A2_MOUSE	67 kDa	6	Neuronal and non-neuronal
110	Nuclear receptor-binding protein OS=Mus musculus GN=Nrbp1 PE=1 SV=1	NRBP_MOUSE	60 kDa	5.25	Neuronal and non-neuronal
111	Obscurin OS=Mus musculus GN=Obscn PE=2 SV=2	OBSCN_MOUSE	966 kDa	2.82	Neuronal and non-neuronal
112	OTU domain-containing protein 6A OS=Mus musculus GN=Otud6a PE=2 SV=1	OTU6A_MOUSE	34 kDa	0.79	Neuronal and non-neuronal
113	PAB-dependent poly(A)-specific ribonuclease subunit 3 OS=Mus musculus GN=Pan3 PE=2 SV=3	PAN3_MOUSE	90 kDa	2.18	Neuronal and non-neuronal
114	Periaxin OS=Mus musculus GN=Prx PE=1 SV=1	PRAX_MOUSE	148 kDa	66.25	Non neuronal
115	Polypeptide N-acetylgalactosaminyltransferase 10 OS=Mus musculus GN=Galnt10 PE=2 SV=1	GLT10_MOUSE	69 kDa	4.25	Neuronal and non-neuronal
116	Potassium channel subfamily U member 1 OS=Mus musculus GN=Kcnu1 PE=1 SV=2	KCNU1_MOUSE	127 kDa	14.375	Non neuronal
117	Potassium voltage-gated channel subfamily E member 1 OS=Mus musculus GN=Kcne1 PE=1 SV=1	KCNE1_MOUSE	15 kDa	2.33	Neuronal and non-neuronal
118	Potassium voltage-gated channel subfamily KQT member 1 OS=Mus musculus GN=Kcnq1 PE=2 SV=3	KCNQ1_MOUSE	75 kDa	24.5	Neuronal and non-neuronal
119	pre-mRNA 3' end processing protein WDR33 OS=Mus musculus GN=Wdr33 PE=2 SV=1	WDR33_MOUSE	145 kDa	1.575	Neuronal and non-neuronal
120	Primary ciliary dyskinesia protein 1 OS=Mus musculus GN=Gm101 PE=1 SV=1	PCDP1_MOUSE	97 kDa	0.95	Neuronal and non-neuronal
121	Probable isocitrate dehydrogenase [NAD] gamma 2, mitochondrial OS=Mus musculus PE=1 SV=1	IDHG2_MOUSE	44 kDa	17.25	Neuronal and non-neuronal
122	Programmed cell death protein 2-like OS=Mus musculus GN=Pdcd2l PE=2 SV=1	PDD2L_MOUSE	40 kDa	0.96	Neuronal and non-neuronal
123	Prohibitin-2 OS=Mus musculus GN=Phb2 PE=1 SV=1	PHB2_MOUSE	33 kDa	0.87	Neuronal and non-neuronal
124	Protein disulfide-isomerase A4 OS=Mus musculus GN=Pdia4 PE=1 SV=3	PDIA4_MOUSE	72 kDa	2.37	Neuronal and non-neuronal
125	Ribonuclease P protein subunit p29 OS=Mus musculus GN=Pop4 PE=2 SV=1	RPP29_MOUSE	26 kDa	8.25	Neuronal and non-neuronal
126	Ribosome biogenesis protein BOP1 OS=Mus musculus GN=Bop1 PE=1 SV=1	BOP1_MOUSE	83 kDa	10	Neuronal and non-neuronal
127	RNA polymerase II-associated protein 1 OS=Mus musculus GN=Rpap1 PE=1 SV=2	RPAP1_MOUSE	155 kDa	9	Neuronal and non-neuronal
128	RNA-binding protein FUS OS=Mus musculus GN=Fus PE=2 SV=1	FUS_MOUSE	53 kDa	6.05	Neuronal and non-neuronal
129	S100P-binding protein OS=Mus musculus GN=S100pbp PE=2 SV=1	S1PBP_MOUSE	44 kDa	1.85	Non neuronal
130	Sacsin OS=Mus musculus GN=Sacs PE=1 SV=2	SACS_MOUSE	521 kDa	1.95	Neuronal
131	SCY1-like protein 2 OS=Mus musculus GN=Scyl2 PE=1 SV=1	SCYL2_MOUSE	103 kDa	1.41	Neuronal and non-neuronal
132	Selection and upkeep of intraepithelial T-cells protein 5 OS=Mus musculus GN=Skint5 PE=2 SV=1	SKIT5_MOUSE	166 kDa	1.22	Non neuronal
133	Serine/threonine-protein kinase receptor R3 OS=Mus musculus GN=Acvrl1 PE=1 SV=2	ACVL1_MOUSE	57 kDa	3.625	Neuronal and non-neuronal
134	Serpin B12 OS=Mus musculus GN=Serpinb12 PE=2 SV=1	SPB12_MOUSE	48 kDa	4.45	Neuronal and non-neuronal
135	Serpin H1 OS=Mus musculus GN=Serpinh1 PE=1 SV=3	SERPH_MOUSE	47 kDa	1.625	Neuronal and non-neuronal
136	Short transient receptor potential channel 2 OS=Mus musculus GN=Trpc2 PE=2 SV=2	TRPC2_MOUSE	131 kDa	11.25	Neuronal and non-neuronal
137	Short-chain dehydrogenase/reductase family 16C member 6 OS=Mus musculus GN=Sdr16c6 PE=2 SV=1	S16C6_MOUSE	35 kDa	1.30	Neuronal and non-neuronal
138	Signal transducer and activator of transcription 2 OS=Mus musculus GN=Stat2 PE=1 SV=1	STAT2_MOUSE	105 kDa	1.02	Neuronal and non-neuronal
139	Small conductance calcium-activated potassium channel protein 2 OS=Mus musculus GN=Kcnn2 PE=2 SV=1	KCNN2_MOUSE	63 kDa	6.5	Neuronal and non-neuronal
140	Sodium/potassium/calcium exchanger 5 OS=Mus musculus GN=Slc24a5 PE=2 SV=1	NCKX5_MOUSE	55 kDa	1.45	Neuronal and non-neuronal
141	Spermatogenesis-associated protein 7 homolog OS=Mus musculus GN=Spata7 PE=2 SV=1	SPAT7_MOUSE	66 kDa	5.75	Neuronal and non-neuronal
142	StAR-related lipid transfer protein 9 OS=Mus musculus GN=Stard9 PE=2 SV=2	STAR9_MOUSE	500 kDa	1.55	Neuronal and non-neuronal
143	Structural maintenance of chromosomes protein 2 OS=Mus musculus GN=Smc2 PE=1 SV=2	SMC2_MOUSE	134 kDa	1.5	Neuronal and non-neuronal
144	Structural maintenance of chromosomes protein 6 OS=Mus musculus GN=Smc6 PE=2 SV=1	SMC6_MOUSE	127 kDa	3.52	Neuronal and non-neuronal
145	SUMO-specific isopeptidase USPL1 OS=Mus musculus GN=Uspl1 PE=2 SV=2	USPL1_MOUSE	118 kDa	8	Neuronal and non-neuronal
146	SWI/SNF-related matrix-associated actin-dependent regulator of chromatin subfamily A containing DEAD/H box 1 OS=Mus musculus GN=Smarcad1 PE=	SMRCD_MOUSE	116 kDa	3.75	Neuronal and non-neuronal
147	Synaptonemal complex protein 2 OS=Mus musculus GN=Sycp2 PE=1 SV=2	SYCP2_MOUSE	172 kDa	0.86	Neuronal and non-neuronal
148	TBC1 domain family member 1 OS=Mus musculus GN=Tbc1d1 PE=1 SV=3	TBCD1_MOUSE	142 kDa	0.75	Neuronal and non-neuronal
149	T-cell receptor beta chain V region PHDS203 (Fragment) OS=Mus musculus PE=4 SV=1	TVB3_MOUSE	14 kDa	0.92	Non neuronal
150	T-complex protein 1 subunit gamma OS=Mus musculus GN=Cct3 PE=1 SV=1	TCPG_MOUSE	61 kDa	0.61	Neuronal and non-neuronal
151	THO complex subunit 2 OS=Mus musculus GN=Thoc2 PE=2 SV=1	THOC2_MOUSE	183 kDa	0.47	Neuronal and non-neuronal
152	Titin OS=Mus musculus GN=Ttn PE=1 SV=1	TITIN_MOUSE	3906 kDa	48.75	Non neuronal
153	T-lymphoma invasion and metastasis-inducing protein 2 OS=Mus musculus GN=Tiam2 PE=1 SV=2	TIAM2_MOUSE	193 kDa	2.12	Neuronal and non-neuronal
154	TRAF family member-associated NF-kappa-B activator OS=Mus musculus GN=Tank PE=1 SV=1	TANK_MOUSE	51 kDa	4.95	Neuronal and non-neuronal
155	Transketolase OS=Mus musculus GN=Tktl1	TKTL1_MOUSE	65 kDa	24.75	Neuronal and non-neuronal
156	Tubulin alpha-1C chain OS=Mus musculus GN=Tuba1c PE=1 SV=1	TBA1C_MOUSE	50 kDa	14.25	Neuronal and non-neuronal
157	Tubulin beta-2A chain OS=Mus musculus GN=Tubb2a PE=1 SV=1	TBB2A_MOUSE	50 kDa	9.12	Neuronal
158	Ubiquitin carboxyl-terminal hydrolase 15 OS=Mus musculus GN=Usp15 PE=2 SV=1	UBP15_MOUSE	112 kDa	1.4	Neuronal and non-neuronal
159	Ubiquitin carboxyl-terminal hydrolase 47 OS=Mus musculus GN=Usp47 PE=1 SV=2	UBP47_MOUSE	157 kDa	0.85	Neuronal and non-neuronal
160	Ubiquitin carboxyl-terminal hydrolase 49 OS=Mus musculus GN=Usp49 PE=2 SV=1	UBP49_MOUSE	78 kDa	2.01	Neuronal and non-neuronal
161	Ubiquitin-60S ribosomal protein L40 OS=Mus musculus GN=Uba52 PE=1 SV=2	RL40_MOUSE	15 kDa	11.25	Neuronal and non-neuronal
162	Uncharacterized protein C11orf35 homolog OS=Mus musculus PE=2 SV=1	CK035_MOUSE	74 kDa	5.91	Neuronal and non-neuronal
163	Uncharacterized protein C4orf51 homolog OS=Mus musculus PE=2 SV=2	CD051_MOUSE	23 kDa	3.39	Neuronal and non-neuronal
164	Vacuolar protein sorting-associated protein 13C OS=Mus musculus GN=Vps13c PE=1 SV=2	VP13C_MOUSE	420 kDa	0.66	Neuronal and non-neuronal
165	Vascular endothelial growth factor receptor 1 OS=Mus musculus GN=Flt1 PE=1 SV=1	VGFR1_MOUSE	150 kDa	11.12	Neuronal and non-neuronal
166	von Willebrand factor A domain-containing protein 1 OS=Mus musculus GN=Vwa1 PE=1 SV=1	VWA1_MOUSE	48 kDa	10.5	Neuronal and non-neuronal
167	Zinc finger protein 382 OS=Mus musculus GN=Znf382 PE=1 SV=1	ZN382_MOUSE	67 kDa	2.69	Neuronal and non-neuronal
168	Zinc finger protein 608 OS=Mus musculus GN=Znf608 PE=2 SV=1	ZN608_MOUSE	162 kDa	1.9625	Neuronal and non-neuronal
169	Zinc finger protein 82 OS=Mus musculus GN=Zfp82 PE=2 SV=1	ZFP82_MOUSE	62 kDa	0.525	Neuronal and non-neuronal

Supplementary table 1 (related to figure 1): Complete overview of the list of putative SUMOylation targets in mouse DRG revealed by LC-MS analyses post-immunoprecipitation with an anti-SUMO1 antibody. See methods for details. Whereever known, we have endeavored to annonate neuronal or non-neuronal origin.

Supplementary table 2 related to figure 1

SN	Identified Proteins	Accession Number	Molecular Weight
	Metabolic enzymes		
1	2-oxoglutarate dehydrogenase, mitochondrial OS=Mus musculus GN=Ogdh PE=1 SV=3	ODO1_MOUSE	115 kDa
2	Acetyl-CoA acetyltransferase, mitochondrial OS=Mus musculus GN=Acat1 PE=1 SV=1	THIL_MOUSE	45 kDa
3	Acyl-coenzyme A thioesterase THEM5 OS=Mus musculus GN=Them5 PE=2 SV=1	ACO15_MOUSE	28 kDa
4	Adenylate cyclase type 10 OS=Mus musculus GN=Adcy10 PE=2 SV=2	ADCYA_MOUSE	186 kDa
5	ADP/ATP translocase 4 OS=Mus musculus GN=Slc25a31 PE=2 SV=1	ADT4_MOUSE	41 kDa
6	Aldehyde dehydrogenase, dimeric NADP-preferring OS=Mus musculus GN=Aldh3a1 PE=2 SV=2	AL3A1_MOUSE	50 kDa
7	Citrate synthase, mitochondrial OS=Mus musculus GN=Cs PE=1 SV=1	CISY_MOUSE	52 kDa
8	Dehydrogenase/reductase SDR family member 1 OS=Mus musculus GN=Dhrs1 PE=2 SV=1	DHRS1_MOUSE	34 kDa
9	Diacylglycerol kinase zeta OS=Mus musculus GN=Dgkz PE=1 SV=2	DGKZ_MOUSE	104 kDa
10	Fructose-bisphosphate aldolase A OS=Mus musculus GN=Aldoa PE=1 SV=2	ALDOA_MOUSE	39 kDa
11	Glyceraldehyde-3-phosphate dehydrogenase OS=Mus musculus GN=Gapdh PE=1 SV=2	G3P_MOUSE	36 kDa
12	Glycogen phosphorylase, brain form OS=Mus musculus GN=Pygb PE=1 SV=3	PYGB_MOUSE	97 kDa
13	Isobutyryl-CoA dehydrogenase, mitochondrial OS=Mus musculus GN=Acad8 PE=2 SV=2	ACAD8_MOUSE	45 kDa
14	L-lactate dehydrogenase B chain OS=Mus musculus GN=Ldhb PE=1 SV=2	LDHB_MOUSE	36 kda
15	L-lactate dehydrogenase C chain OS=Mus musculus GN=Ldhc PE=1 SV=2	LDHC_MOUSE	36 kDa
16	Malate dehydrogenase, mitochondrial OS=Mus musculus GN=Mdh2 PE=1 SV=3	MDHM_MOUSE	35 kDa
17	NAD(P) transhydrogenase, mitochondrial OS=Mus musculus GN=Nnt PE=1 SV=2	NNTM_MOUSE	114 kDa
18	NADH-ubiquinone oxidoreductase 75 kDa subunit, mitochondrial OS=Mus musculus GN=Ndufs1 PE	NDUS1_MOUSE	80 kDa
19	Polypeptide N-acetylgalactosaminyltransferase 10 OS=Mus musculus GN=Galnt10 PE=2 SV=1	GLT10_MOUSE	69 kDa
20	Probable isocitrate dehydrogenase [NAD] gamma 2, mitochondrial OS=Mus musculus PE=1 SV=1	IDHG2_MOUSE	44 kDa
21	Short-chain dehydrogenase/reductase family 16C member 6 OS=Mus musculus GN=Sdr16c6 PE=2	S16C6_MOUSE	35 kDa
22	Transketolase OS=Mus musculus GN=Tktl1	TKTL1_MOUSE	65 kDa
23	3-ketoacyl-CoA thiolase, mitochondrial OS=Mus musculus GN=Acaa2 PE=1 SV=3	THIM_MOUSE	41 kDa
24	Aspartate aminotransferase, mitochondrial OS=Mus musculus GN=Got2 PE=1 SV=1	AATM_MOUSE	47 kDa
25	Cytochrome b-c1 complex subunit 2, mitochondrial OS=Mus musculus GN=Uqcrc2 PE=1 SV=1	QCR2_MOUSE	48 kDa
26	Cytoplasmic aconitate hydratase OS=Mus musculus GN=Aco1 PE=1 SV=3	ACOC_MOUSE	98 kDa
27	Dihydrolipoyllysine-residue acetyltransferase component of pyruvate dehydrogenase complex, mitoc	ODP2_MOUSE	68 kDa
28	Delta-1-pyrroline-5-carboxylate synthase OS=Mus musculus GN=Aldh18a1 PE=2 SV=2	P5CS_MOUSE	87 kDa
	Ion channels		
1	Potassium channel subfamily U member 1 OS=Mus musculus GN=Kcnu1 PE=1 SV=2	KCNU1_MOUSE	127 kDa
2	Potassium voltage-gated channel subfamily E member 1 OS=Mus musculus GN=Kcne1 PE=1 SV=1	KCNE1_MOUSE	15 kDa
3	Potassium voltage-gated channel subfamily KQT member 1 OS=Mus musculus GN=Kcnq1 PE=2 SV	KCNQ1_MOUSE	75 kDa
4	Short transient receptor potential channel 2 OS=Mus musculus GN=Trpc2 PE=2 SV=2	TRPC2_MOUSE	131 kDa
5	Sodium/potassium/calcium exchanger 5 OS=Mus musculus GN=Slc24a5 PE=2 SV=1	NCKX5_MOUSE	55 kDa
6	Small conductance calcium-activated potassium channel protein 2 OS=Mus musculus GN=Kcnn2 PE	KCNN2_MOUSE	63 kDa
	Heat shock proteins		
1	Heat shock 70 kDa protein 12A OS=Mus musculus GN=Hspa12a PE=1 SV=1	HS12A_MOUSE	74 kDa
2	Heat shock cognate 71 kDa protein OS=Mus musculus GN=Hspa8 PE=1 SV=1	HSP7C_MOUSE	71 kDa
3	Heat shock protein HSP 90-alpha OS=Mus musculus GN=Hsp90aa1 PE=1 SV=4	HS90A_MOUSE	85 kDa
4	Heat shock protein HSP 90-beta OS=Mus musculus GN=Hsp90ab1 PE=1 SV=3	HS90B_MOUSE	83 kDa
5	78 kDa glucose-regulated protein OS=Mus musculus GN=Hspa5 PE=1 SV=3	GRP78_MOUSE	72 kDa
	Other enzymes		
1	1-phosphatidylinositol 4,5-bisphosphate phosphodiesterase zeta-1 OS=Mus musculus GN=Plcz1 PE	PLCZ1_MOUSE	75 kDa
2	Alpha-N-acetylneuraminide alpha-2,8-sialyltransferase OS=Mus musculus GN=St8sia1 PE=1 SV=2	SIA8A_MOUSE	40 kDa
3	Arf-GAP with SH3 domain, ANK repeat and PH domain-containing protein 2 OS=Mus musculus GN=	ASAP2_MOUSE	107 kDa
4	ATP-dependent DNA helicase Q4 OS=Mus musculus GN=Recql4 PE=2 SV=2	RECQ4_MOUSE	135 kDa
5	Cytosolic carboxypeptidase 4 OS=Mus musculus GN=Agbl1 PE=1 SV=2	CBPC4_MOUSE	109 kDa
6	Death-associated protein kinase 1 OS=Mus musculus GN=Dapk1 PE=1 SV=3	DAPK1_MOUSE	161 kDa
7	DNA helicase MCM9 OS=Mus musculus GN=Mcm9 PE=1 SV=2	MCM9_MOUSE	126 kDa
8	Dual specificity protein kinase CLK3 OS=Mus musculus GN=Clk3 PE=1 SV=2	CLK3_MOUSE	74 kDa
9	Exonuclease 1 OS=Mus musculus GN=Exo1 PE=2 SV=2	EXO1_MOUSE	92 kDa
10	Heparan-sulfate 6-O-sulfotransferase 2 OS=Mus musculus GN=Hs6st2 PE=2 SV=3	H6ST2_MOUSE	69 kDa
11	N6-adenosine-methyltransferase 70 kDa subunit OS=Mus musculus GN=Mettl3 PE=2 SV=2	MTA70_MOUSE	65 kDa
12	Nitric oxide synthase, brain OS=Mus musculus GN=Nos1 PE=1 SV=1	NOS1_MOUSE	160 kDa
13	Protein disulfide-isomerase A4 OS=Mus musculus GN=Pdia4 PE=1 SV=3	PDIA4_MOUSE	72 kDa
14	SUMO-specific isopeptidase USPL1 OS=Mus musculus GN=Uspl1 PE=2 SV=2	USPL1_MOUSE	118 kDa
15	Ubiquitin carboxyl-terminal hydrolase 15 OS=Mus musculus GN=Usp15 PE=2 SV=1	UBP15_MOUSE	112 kDa
16	Ubiquitin carboxyl-terminal hydrolase 47 OS=Mus musculus GN=Usp47 PE=1 SV=2	UBP47_MOUSE	157 kDa
17	Ubiquitin carboxyl-terminal hydrolase 49 OS=Mus musculus GN=Usp49 PE=2 SV=1	UBP49_MOUSE	78 kDa

Supplementary table 2 (related to figure 1): Overview of putative SUMOylation targets with their known functional annotations.

Supplementary table 3 related to figure 1

S.N	Identified Proteins	Accession Number	Non-diabetic	Diabetic
1	Aspartate aminotransferase, mitochondrial	AATM		
2	Aldehyde dehydrogeanse, dimeric NADP	AL3A1		
3	Fructose-bisphosphate aldolase A	ALDOA		
4	Citrate synthase	CISY		
5	Dehydrogenase/reductase SDR family member 1	DHRS1		
6	Glyceraldehyde-3-phosphate dehydrogeanse (GAPDH)	G3P		
7	Dihydrolipoyllysine-residue acteyltransferase	ODP2		
8	Glycogen phosphorylase brain form	PYGB		
9	Cytochrome b-c1 complex subunit 2, mitochondrial	QCR2		
10	Heat shock 70 Kda protein 12A	HS12A		
11	Heat shock protein 90-alpha	HS90A		
12	Heat shock protein 90-beta	HS90B		
13	Malate dehydrogeanse, mitochondrial	MDHM		
14	NADH-ubiquinone oxidoreductase	NDUS1		
15	2-oxoglutarate dehydrogeanse, mitochondrial	ODO1		
16	D-3-phosphoglycerate dehydrogenase	SERA		
17	Acetyl-CoA acetyltransferase, mitochondrial	THIL		
18	3-ketoacyl-CoA thiolase, mitochondrial	THIM		
19	Isobutyryl-CoA dehydrogenase, mitochondrial	ACAD8		
20	Acetyl-coenzyme A thioesterase THEM5	ACO15		
21	78 Kda glucose-regulated protein	GRP78		
22	Probable isocitrate dehydrogenase (NAD) gamma2	IDHG2		
23	L-lactate dehydrogeanse C chain	LDHC		
24	NAD(P) transhydrogenase, mitochondrial	NNTM		
25	Hydroxymethylglutaryl-CoA synthase, mitochondrial	HMCS2		
26	Mitchondrial coenzyme A transporter SLC25A42	S2542		
27	ADP/ATP tarnslocase 4	ADT4		
28	FAD-dependent oxidoreductase domain-containing protein	FXRD1		
29	Potassium voltage-gated channel subfamily KQT	KCNQ1		
30	Ornithine decarboxylase antienzyme 1	OAZ1		
31	Sodium channel protein type 11 subunit alpha	SCNBA		
32	Transketolase	TKTL1		

Supplementary table 3 (related to figure 1): Overview of putative SUMOylation targets that were differentially immunoprecipitated in DRG samples from mice injected with Streptozotocin (STZ, 5 weeks) and age-matched nondiabetic controls. Please note that these analyses are not quantitative in nature.

Supplementary table 4 related to figure 1

Name	SUMOsp 2.0		SumoPLOT
	high	low	Probability
Trp Channels			
Trpa1	++(1)	+++(6)	0.85(11)
Trpc6	++(2)	+++(3)	0.94(5)
Trpc3	++++(3)	++++(6)	0.94(9)
Trpv1	++(2)	+++(3)	0.91(8)
Trpc4	+++++(4)	+++++(8)	0.91(12)
Trpm3	+++++(6)	+++++(14)	0.93(24)
Trpv2	N	N	0.73(7)
Trpm4	N	++++(3)	0.61(6)
Sodium channels			
Scn10a	+(1)	+++(12)	0.8(23)
Scn11a	+(1)	+++(11)	0.94(24)
Scn2b	++(2)	++++(5)	0.91(5)
Scn3b	+(1)	++++(2)	0.8(2)
Scn9a	++++(3)	++++(20)	0.93(22)
Calcium channels			
Cacna2d1	++(2)	++(2)	0.94(12)
Cacna1b	+(2)	++++(12)	0.85(22)
Cacna1c	++++(3)	+++++(12)	0.94(12)
Cacn1b	N	++++(3)	0.93(4)
Cacnb3	++++(1)	++++(3)	0.91(3)

+	0 - 1
++	1 - 2
+++	2 - 3
++++	3 - 4

Supplementary table 4 (related to figure 1): Overview of ion-channels belonging to 3 major families linked to sensory properties of DRG neurons that were found to harbor motifs for SUMOylation in in silico analyses (SUMOSP 2.0 and SUMOPLOT). The number of potentially SUMOylated lysine residues is given in brackets, and the score assigned by SUMOSP 2.0 and and calculated probability of SUMOylation given by SUMOPLOT are indicated. N indicates ‘not found’.

List of primary antibodies			
Antibody	**Source**	**Dilution**	**RRID**
Rat anti-HA	Roche	1:500 (IB); 1:75 (IF)	AB_390919
Rabbit anti-HA	Cell signaling	1.1000 (IB)	AB_10693385
Mouse anti-HA	Covance	1:100 (IF)	AB_291259
Mouse anti-Sumo1	DSHB	1:1000 (IB)	AB_2198257
Mouse anti-GFP	DSHB	1:700 (IB)	AB_2617419
Rabbit anti-GAPDH	Thermo Scientific	1:1000 (IB)	AB_568552
Rabbit anti-tubulin	Sigma Aldrich	1:4000 (IB)	AB_261659
Rabbit anti-TKTL1	Sigma Aldrich	1:500 (IB)	AB_10665408
Rabbit anti-citrate synthase	Thermo Scientific	1:1000 (IB)	AB_2787810
Mouse anti-ALDH	Origene	1:1500 (IB)	AB_10774056
Rabbit anti-pgp9.5	Dako	1:1000 (IF)	AB_2622233
Rabbit anti-NF200	Sigma Aldrich	1:300 (IF)	AB_477272
Biotinylated Griffonia simplicifolia Isolectin-B4 (IB4)	Vector lab	1:200 (IF)	AB_2314661
Rabbit anti-FLAG	Sigma Aldrich	1:1000 (IB)	AB_2811010
Rabbit anti-CGRP	Immuno star	1:2000 (IF)	AB_572217
Goat anti-Ubc9	Santa Cruz	1:50 (IF)	AB_2256740
Rabbit anti-GFP	Sigma Aldrich	IP	AB_2750576

List of secondary antibodies			
Antibody	**Source**	**Dilution**	**RRID**
Donkey anti rabbit-Alexa Fluor 488	Invitrogen	1:500	AB_2762833
Donkey anti-rabbit-Alexa Fluor 594	Invitrogen	1:500	AB_2762827
Donkey anti-goat-Alexa Fluor 488	Invitrogen	1:500	AB_2762838
Streptavidin-Alexa Fluor 594	Invitrogen	1:500	AB_2315780
Anti-mouse-HRP	GE healthcare	1:4000	AB_772210
Anti-rabbit-HRP	Sigma Aldrich	1:4000	AB_772206
Anti-goat-HRP	Santa Cruz	1:4000	AB_631728

Supplementary table 5 (related to star methods): List of the antibodies with working dilutions and applications.